Multidisciplinary Conceptual Design for Reduced-Emission Rotorcraft

Christopher Silva **Wayne Johnson**
NASA Ames Research Center
Moffett Field, CA, USA

Eduardo Solis
Science and Technology Corporation
Moffett Field, CA, USA

ABSTRACT

Python-based wrappers for OpenMDAO are used to integrate disparate software for practical conceptual design of rotorcraft. The suite of tools which are connected thus far include aircraft sizing, comprehensive analysis, and parametric geometry. The tools are exercised to design aircraft with aggressive goals for emission reductions relative to fielded state-of-the-art rotorcraft. Several advanced reduced-emission rotorcraft are designed and analyzed, demonstrating the flexibility of the tools to consider a wide variety of potentially transformative vertical flight vehicles. To explore scale effects, aircraft have been sized for 5, 24, or 76 passengers in their design missions. Aircraft types evaluated include tiltrotor, single-main-rotor, coaxial, and side-by-side helicopters. Energy and drive systems modeled include Lithium-ion battery, hydrogen fuel cell, turboelectric hybrid, and turboshaft drive systems. Observations include the complex nature of the trade space for this simple problem, with many potential aircraft design and operational solutions for achieving significant emission reductions. Also interesting is that achieving greatly reduced emissions may not require exotic component technologies, but may be achieved with a dedicated design objective of reducing emissions.

BACKGROUND

Traditional conceptual design methods rely on parametric relations and simplified analyses implemented in either very specific and inflexible or in broad and under-validated design tools. Novel designs impel designers to explore regions outside of the "truth" dataset's domain of validity, and to perhaps connect components in ways that may not lend themselves to traditional solution procedures. Design space exploration is a critical part of conceptual design, and with new types of aircraft come new complexities with regard to aircraft topology, interactions among components, and methods of operation.

The added complexity of these degrees of freedom can overwhelm a design team, leading to a premature culling of the aircraft types from consideration and therefore limiting the search of a solution space to the topologically connected region of a local optimum rather than a more globally optimal solution. For instance, a mission may be completed by several different types of rotorcraft, with variable numbers of main rotors (single main rotor helicopters, coaxial helicopters, etc.), or with tilting rotors and wings. Each type of aircraft will have its own design space topology, with discontinuities and regions of infeasibility, and the overall design space will almost certainly have discontinuities when going between different types of aircraft.

A goal of the present tool development effort within NASA's Revolutionary Vertical Lift Technologies program is to provide robust tools, which facilitate design space exploration with varied problem definitions and with the ability to concurrently consider several different potential solutions. A second goal is to speed the setup and execution of design space exploration, specifically for vertical lift aircraft designed to objective functions other than minimization of acquisition or operating cost. The tools and examples developed in the present research will be made available to other researchers to serve as starting points for their own design studies and technology maturation efforts.

The NASA Design and Analysis of Rotorcraft (NDARC) software tool (Ref. 1) has been designed from the outset with flexibility to design and analyze a large variety of aircraft, yet many of its underlying empirical models are limited by their basis in historic aircraft data. A solution to this limitation is to separate the design and analysis procedures into those which are performed by the monolithic design tool and those which are performed by interconnected tools which are capable of returning results for their domain of applicability with the information available at the conceptual design stage. This is the solution which we have implemented in the present study. Tools exist to model and analyze a wide variety of rotor-

AHS Specialists Conference on Aeromechanics Design for Transformative Vertical Flight, San Francisco, California, USA, January 16-18, 2018.

craft and their subsystems with a high degree of confidence, but the level of detail required and time consumed setting up and performing these analyses has been prohibitive for broad-scoped conceptual design. This desire to rapidly connect disparate analyses into different problem formulations leads to a need for a robust platform for software integration which leverages code reuse and abstraction of common solution and execution functions through a consistent application programming interface. OpenMDAO (Ref. 2) version 1.7 is such a tool, with a well-defined application programming interface and the ability to solve problems which involve gradient and gradient-free solution procedures for a hierarchically-defined optimization problem.

Multidisciplinary design, analysis, and optimization (MDAO) is a field of active research, with researchers establishing best practices for balancing increasing fidelity and minimizing turn-around time. An additional promise of MDAO is the possibility to uncover non-intuitive solutions, by utilizing multidisciplinary tools to model complex couplings and nonlinearities.

The NASA Aeronautics Strategic Implementation Plan (Ref. 3) has outlined development of tools for industrial, academic, and government researchers to use, and also the development of conceptual design aircraft which quantify technology payoff and establish the potential of new types of vertical lift aircraft. The objective of this present paper is to illustrate the use of these tools to design aircraft which may perform vertical lift missions with large reductions in emissions. The air vehicle predictions in this study are constrained to remain within the bounds of technology which can credibly be estimated for entry into service within the next decade, meaning that some energy storage and conversion mechanisms with little or no experimental basis or industrial capacity are not presently considered. This work illustrates how NDARC and other tools can contribute toward confident development and investment decisions, including cases with advanced technology and unusual aircraft attributes.

APPROACH

Several types of aircraft with varying energy storage and drive system topologies are modeled in order to exercise the tools and methods across a wide set of possible aircraft. Various types of vehicles are designed for two size classes of traditional rotorcraft missions and one non-traditional rotorcraft mission (served today by regional turboprops). For these vehicles, power trains considered include jet fuel turboshaft, battery electric motor, and hydrogen fuel cell electric motor for energy storage and conversion.

Optimization is performed to reduce emissions relative to a baseline aircraft which has been designed with calibration factors representing today's fielded state-of-the-art. The optimization driver is allowed to vary parameters for which NDARC or the comprehensive analysis has an input, such as cruise altitude, rotor tip speed, wing loading, and disk loading. The target for emissions reduction is 50% reduction relative to the baseline aircraft on the design mission, with the expectation that some of the reduction comes from aerodynamic and structural efficiency, and some reduction might come from improvements in propulsion systems. The metrics selected for emissions are both related to long-term climate change impacts of aviation, the Emissions Trading Scheme (ETS) and Average Temperature Response (ATR) metrics, which have been integrated into NDARC version 1.11, and which has been exercised for similar design objectives in (Ref. 4).

The purpose of this study was not to forecast where a particular low-emission technology or vehicle type would be best in an absolute sense, but rather to explore how advances in technology could be used to provide similar capabilities to those available today, with emissions reduced by 50% or more. As a result, some technologies and design approaches which drastically reduce emissions were not explored in depth, because the resultant vehicles either cannot perform the missions, or perform the mission with a vehicle so large and expensive that it would not be economically competitive.

Due to the flexibility of NDARC and the immense complexity which arises from considering various types of aircraft, the design process first begins with a manually-designed "seed" aircraft which is itself a feasible solution to the mission requirements. This aircraft may then be modified by an optimizer to adjust the design vector and perform design iterations until the objective function is optimized or the number of allowed iterations are expended. The overall process is depicted in Figure 1. The traditional design process inside box with thick black border generates the seed, and the optimizer will eventually interact with all of the items in blue boxes.

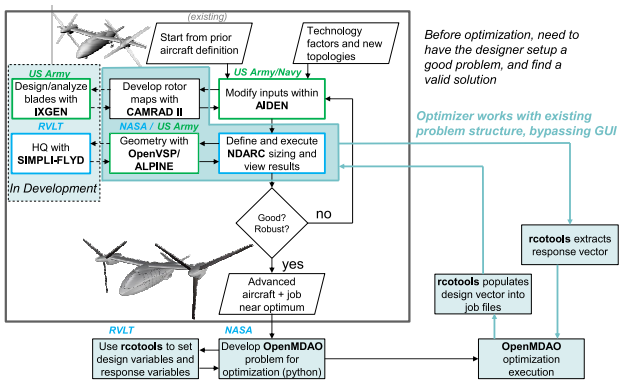

Fig. 1. Optimization improves on an initial design

The aircraft design is initialized from a previous aircraft definition for NDARC (if possible, for rapidity of setup), with changes made to the inputs in text files and through a graphical user interface (AIDEN, (Ref. 5)). A set of technology factor inputs are applied through AIDEN to NDARC, with each of these factors generated by first calibrating to a technology factor of a relevant existing aircraft or component (if possible) or by analysis. This includes choosing which parametric model is most applicable (e.g. the wing weight models available in NDARC include fixed areal density, empirical

fixed-wing, and semi-analytical tiltrotor models). Technology improvements with a basis in research (the preferred approach) or fiat (for technology goals) are then applied to the calibration technology factor to arrive at the net technology factor used by NDARC. In the graphic shown here, a tiltrotor with wing extensions and 4 blades per rotor has been modified by the user to eliminate the wing extensions and change the number of rotor blades. The current method of modeling a tiltrotor with wing extensions involves several input parameters for structures and aerodynamics in the wing and nacelle models, in addition to changes in wing sizing parameters; expert user intervention is required to enact this type of change.

Comprehensive analysis is performed using CAMRAD II (Ref. 6) to generate rotor surrogate model parameters, and those are used in vehicle sizing and analysis within NDARC. The rotor is optimized for a combination of hover and forward flight performance which matches flight conditions in the design mission, by varying airfoils, taper, sweep, and twist.

NDARC performs vehicle sizing based on specified design missions and conditions. Each NDARC run generates output which is used by OpenVSP (Ref. 7) through ALPINE (Ref. 8) to create parametric geometry which is checked for consistency of wetted areas, layout and mass properties. A closed design is reached through a fixed point iteration between NDARC and OpenVSP. In the current implementation of ALPINE, OpenVSP geometry is generated by reading NDARC "geometry" and "design" output files, which then generate ALPINE geometry objects, and those in turn generate and manipulate OpenVSP primitives which include standard and custom components. ALPINE also generates a mass representation of the vehicle, which may be used for verifying weight and balance, and as inertial properties for flight control simulation. The initial pass through design with ALPINE/OpenVSP creates a rather generic rotorcraft using custom geometry scripts for the components. Fig. 2 depicts the process of using the OpenVSP geometry with Rhino3D to improve layout, aesthetics, and create smooth, water-tight geometry suitable for CFD analysis.

Typical geometric additions include fairings, placement of transparencies and access doors and panels, and complex curvature. Placement of internal components such as engine inlet and exhaust paths, drive shafts, and structural components, have not yet been implemented in the parametric geometry generation of ALPINE, necessitating the manual layout work here. The modified geometry may then be used to adjust the OpenVSP model for future parametric design work.

The NDARC job file for the closed design is then used as the basis for optimization. RCOTools (Ref. 9) utilities are used to identify design and response variables,

A python script is then written to define the execution topology, then perform the optimization using OpenMDAO, which uses the RCOTools wrappers to control execution of NDARC and CAMRAD II, and to query the response vectors.

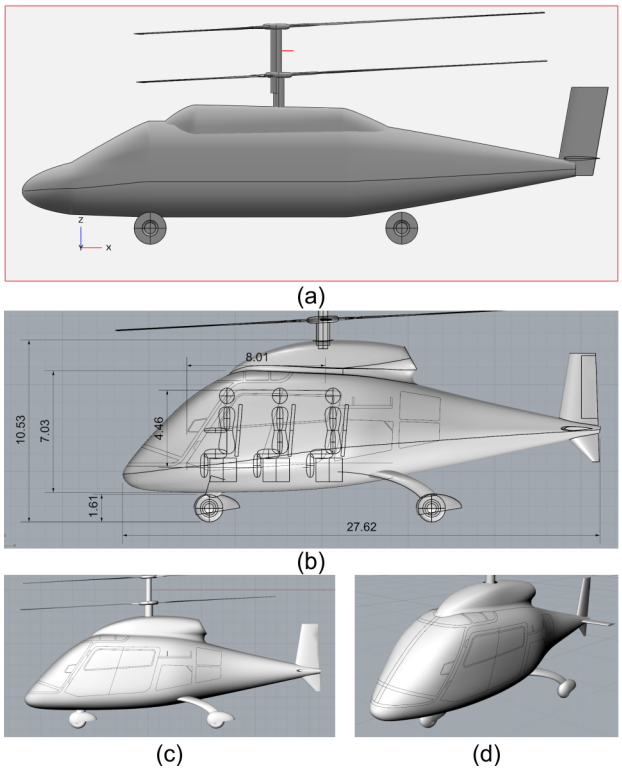

Fig. 2. Geometry definition progresses from (a) initial ALPINE/OpenVSP graphic, through (b) layout checks for consistency and styling of fuselage, to (c and d) geometry for visualization and CFD

Software Tools Developed for this Study

The primary software tool used for design is NDARC version 1.11 (as of publication, version 1.12 is the current version), which includes some specific improvements related to this work. Vehicle sizing and analysis is performed in a manner consistent with NDARCs traditional usage. NDARC is distributed with several example cases to help users determine how to build new aircraft models and design or analyze them, and these were used in this study; the resultant models from this study will be provided as example cases for future use. A specific module is implemented in NDARC for emissions modeling of the Emissions Trading Scheme (ETS) and the Average Temperature Response (ATR), in addition to several constituent emission components. Turboshaft emissions for the ETS metric (kg of CO_2) are directly related to fuel burn. The ATR metric includes as a primary component the kg of CO_2 generated, but includes other components as well, including NO_x and Aviation Induced Cloudiness.

The hydrogen fuel cell module in NDARC is updated and improved. NDARC was also modified to allow for the sizing of generator components in hybrid propulsion schemes such as series turboelectric systems.

A new Python-based package, RCOTools, performs the functions of wrapping NDARC, CAMRAD II, and it is currently being extended to include the engine analysis tool NPSS. RCOTools manages the interface between the rotorcraft tools and OpenMDAO, which executes the design space

exploration through optimization drivers and has interfaces for other software which may be used in a multidisciplinary study. RCOTools includes several example cases in order to help the designer set up initial cases of their own. SIMPLIFLYD (Ref. 10) is used to perform design of a flight control system based on NDARC and ALPINE inputs, but it has not yet been integrated into the overall automated optimization framework. For rotor blade and other high-aspect-ratio structures, IXGEN has been used, and is also not yet integrated into the optimization framework. IXGEN (Ref. 11) is a GUI for University of Michigan VABS beam analysis software, and has a Python interface to allow use with RCOTools and OpenMDAO version 1.x.

Design Missions and Conditions

Reference design missions for three classes have been developed, with a graphical depiction of a generic design mission in Figure 3. The three classes of vehicles selected for this study cover a broad selection of payloads and distances. A vehicle "class" in our present usage refers to the set of missions and conditions which size (design) the vehicle.

These missions roughly approximate current aircraft markets/niches and for which there are existing aircraft with similar capabilities which we can use as comparisons for each to ensure that we are capturing technologies and equipage correctly.

Item 1 in the figure is an initial taxi segment to ensure that the fuel tank or battery is sized for ground maneuvers. Item 2 is a hover out of ground effect for 5 minutes at an atmosphere of 5,000 ft pressure altitude and 77.2 ^{o}F (ISA + 20 ^{o}C), which ensures that a hover capability is present in the aircraft and that an appreciable amount of energy is expended in hover, without dominating mission energy required. Item 3 is a climb segment in an ISA atmosphere at best climb speed and with a limit of Intermediate Rated Power (30-minute; IRP). Item 4 is a cruise at long range cruise speed (99% of peak specific range, high side, V_{LRC}) at the "best" altitude in an ISA atmosphere, subject to a constraint on altitude due to pressurization requirements or capabilities. The asterisk in the graphic is a note to indicate that the cruise segments were modeled as 4 or 5 segments, so that as the cruise segments for conforming vehicles were compared to those unable to perform the full range, a consistent plot of energy burn could be generated (see Results section). "Best" altitude is a design variable, set by the optimizer, and varies with different objective functions. Item 5 is a descent and landing, which is not flown in this mission analysis. The initial hover accounts for the fuel burn, and descent fuel burn is typically not considered for sizing. Since the final hover is at the takeoff altitude, and for each propulsion system considered in this study the weight of the aircraft is either constant or decreasing over the course of the mission, this is not a power sizing segment. Item 6 is a 30 minute reserve segment, flown at best endurance speed (minimum fuel/energy flow, V_{BE}). Segments 1-4 contribute to mission fuel or mission energy. Alternately, 10% of mission fuel is held in reserve if this value is greater than that consumed in the 30 minute reserve segment.

The smallest vehicle category, Class A, is a 4-6 passenger aircraft capable of 400 nm mission range. This roughly corresponds to the smallest passenger air service vehicles in commercial use today, flying missions including sightseeing, emergency medical services, and personnel transport. The second category, Class B, is a 24-passenger aircraft capable of 500 nm mission range. This corresponds to large passenger helicopters today, often used for offshore personnel transport. The third category, Class C, is a 76-passenger aircraft capable of 1300 nm mission range. This capability is in line with regional fixed-wing transport aircraft in the United States, where mainline airline pilot labor agreements limit maximum takeoff weight and passenger count of aircraft flown by regional partner airlines (often referred to simply as the "scope clause"). While this is a nontraditional VTOL mission, we have included it here as a continuation of recent research into large civil tiltrotors. The capability embodied by Class C is slightly smaller than the NASA LCTR2 (Ref. 12), which is intended to be capable of transporting 90 passengers and has been studied extensively over the past decade.

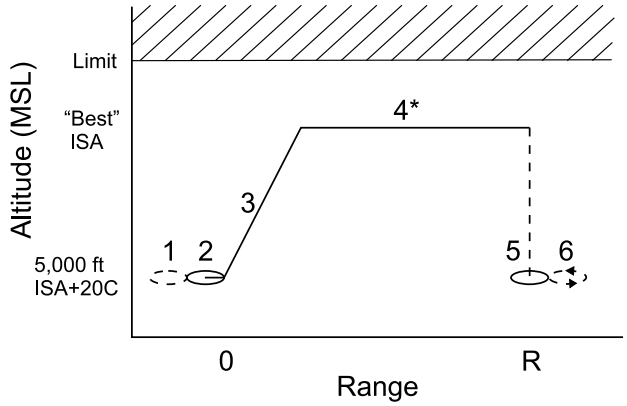

Fig. 3. General Mission Description

Table 1. Design Missions and Parameters

Parameter	Units	Class A	Class B	Class C
OEI rule	–	AI>1.5	Cat. A	Cat. A
OEI speed	KTAS	N/A	30	30
Crew	–	1	3	5
Passengers	–	5	24	76
Range	nm	400	500	1300

Technologies

For baseline vehicles, technology factors, aerodynamics, and fuel consumption are representative of aircraft in current civilian usage; baseline technology can be considered to be Technology Readiness Level (TRL) of 9 (Ref. 13). For the advanced technology vehicles, a set of technology factors based upon the expected technology for a new-start aircraft to

be fielded in the mid-2020s has been selected. The authors have accepted technologies with a TRL of 5 (by our own assessment) or greater as being available for consideration for the advanced technology vehicles, with preference for technologies which are on track for TRL 6 demonstration by 2020 (such as in the Joint Multirole Technology Demonstration program (Ref. 14)). In the cases of battery and fuel cell technologies, the specific energy and power are close to the best demonstrated in laboratory settings, with the assumption that this level may be industrialized within the next decade. A consistent application of technology factors and related inputs must be specified by the designer when setting up the seed vehicles, and can only be modified in the course of optimization as the output of a higher-fidelity discipline analysis.

Engine Technology

The engine models used for the baseline aircraft are typical of existing state-of-the-art and are the generic engines included with the standard NDARC examples distribution. Advanced engine technology in turboshafts provides improvements in specific fuel consumption, specific power, and the production of NO_x in the exhaust. The Class B and Class C vehicles benefit from advancements such as delivered by the AATE/ITEP, FATE, and VAATE engine technology programs. No advancements in the reduction of contrail formation have been applied, but as shall be seen in the case of the tiltrotor, this may be a valuable course of research when considering the atmospheric impact of Aviation Induced Cloudiness, especially as represented in the ATR model.

Battery Technology

Batteries for this study have characteristics of Lithium-ion batteries, as modeled in NDARC. The battery model accounts for discharge rate and state of charge degradation in cell voltage delivered. The missions and aircraft sizes for the present study required very advanced battery technology to result in reasonably-sized aircraft, even at the 100 nm minimum allowed range. A cell-level specific energy of 650 Wh/kg (as compared to current technology around 200 Wh/kg), with an 80% usable capacity was assumed for advanced technology, yielding 520 Wh/kg (1.87 MJ/kg) usable (80%), after applying margins on maximum and minimum state of charge. Battery CO_2 production is based upon the average U.S. estimate for grid-delivered electricity of 0.14 kg CO_2 per MJ.

Fuel Cell Technology

Fuel cells which consume hydrogen gas with a proton exchange membrane have been considered as an alternative energy source to reduce emissions, due to their low specific fuel consumption and exhaust consisting solely of water vapor. The fuel cell model has been updated from the initial NDARC version 1.11 model, to correct some deficiencies and better model proton exchange membrane fuel cells, and both the final 1.11 release and the version 1.12 releases incorporate these changes. For the vehicles and missions in the present study, specific power of fuel cells is the most limiting factor for feasibility. Current technology is represented by specific power of 2.68 lb/hp, and advanced technology is represented by 1.45 lb/hp. Despite this advanced technology, mission ranges had to be reduced to arrive at comparably sized aircraft.

Fuel cell CO_2 emissions are calculated by using the amount of CO_2 produced to generate H_2 in current industrial practice. Our estimate is based upon the current state of H_2 production in the United States, 95% of which comes from steam methane reforming (Ref. 15), and a modern plant (Ref. 16) generates 25,000 lb of CO_2 per 1 million standard cubic feet of H_2, or 4.8 kg CO_2 per kg H_2. As with Jet A, the extraction, refining, and transport emissions are not included in the total emissions estimate.

Rotor Technology

For baseline aircraft, rotor performance represents the most advanced production rotorcraft today, with good passive rotors having advanced airfoils, sweep, and taper, and unfaired hubs. For advanced technology aircraft, the main rotor hub drag coefficient has been reduced by 40%, from 0.0025 to 0.0015 to represent improvements due to passive fairing of hubs.

Drive System Technology

Advanced drive systems for rotorcraft have been the subject of multiple research efforts, with some recent TRL6 demonstrations of integrated gearboxes (Ref. 17). The advanced drives systems in the present study represent the application of advanced metals, torque splitting and topology optimization, and supercritical composite shafts. For the High Efficiency Civil Tiltrotor, the main gearbox case weight has been reduced by splitting torque delivery from thrust- and moment-reaction; the gearbox delivers torque and the nacelle structure reacts thrust and moment from the rotors. The HECTR also has a two-speed transmission. Additionally, there is no conventional "rotor shaft" in the HECTR, with a direct connection from the gearbox/nacelle to the hub. These HECTR drive system features are currently being prepared for TRL 5/6 demonstrations (Ref. 18).

Structures Technology

Advanced technology structures generally represent composite materials and large, co-cured assemblies where applicable.

Instruments, Avionics and Furnishings

Equipage for the baseline and advanced technology aircraft are assumed to have the same weight allocation that a current aircraft with instrument flight capability would have.

Energy and Propulsion Schemes

For hydrocarbon (Jet-A) fueled turboshaft engines, single- and multi-speed transmissions are examined, with significant rotor and engine efficiencies possible by selecting appropriate hover and cruise speeds for the rotors and engines. Turbo-electric serial hybrid is examined, with a parallel battery storage in order to match the power required for hover and cruise in order to keep the turboshaft operating near peak efficiency. Lithium-ion batteries are examined as a primary energy storage source, with significant reductions in emissions possible, but with much lower energy density than jet fuel. Hydrogen fuel cells are examined, with significant reductions in emissions, but a fairly low specific power capability compared to turboshaft engines.

Aircraft Types

Several different types of rotorcraft (where "type" here refers to an aircrafts general arrangement of rotors, propulsors, and wings; other authors have applied "configuration" for this purpose) have been selected to represent some of the features and characteristics of viable aircraft which may meet the mission goals in a reasonable size. Another reason for considering various types of aircraft is the expectation that different types of aircraft may be inherently better suited for emission reduction through increases in efficiency. For the baseline vehicles, single main rotor helicopters have been selected for Class A (Figure 20) and Class B (Figure 24), and a conventional tiltrotor (Figure 29) is representative of Class C.

As discussed in the Technologies section above, the baseline vehicles are designed with fielded state-of-the-art technology for structures, aerodynamics, and propulsion. For each of the baseline vehicles, an advanced technology version has also been designed, to isolate the impact of technology insertion. In addition to these advanced technology aircraft of the conventional types of aircraft, several different advanced technology aircraft of a more unconventional type have been modeled.

The single main rotor (SMR) helicopter is a very common type of aircraft in all helicopter markets, and thus makes a logical baseline for application of technology and as a comparison to different types of aircraft. The Class A SMR aircraft (Fig. 20) has fixed landing gear, and we opted for wheels rather than skids as a designer's choice. The wheels and supports are faired in the advanced technology aircraft, and this follows practice for fixed wing aircraft of similar speed. For Class B (Fig. 24), the wheels are retractable, which matches the practice of other vehicles in the field in this size class, such as AgustaWestland AW139 and Sikorsky S-92. The baseline helicopters are largely aluminum, but have a significant composite content.

The baseline tiltrotor (TR, Fig. 29) employs the design approach and technologies that the Bell-Boeing V-22 and AgustaWestland AW609 have taken. The rotor system is a 3-blade gimballed rotor, and the wing has a very thick airfoil (23%) for aeroelastic stability. The baseline tiltrotor is largely composite, following the practice of V-22 and AW609.

A coaxial helicopter (CX) is a candidate vehicle for reduced emissions, with good hover efficiency, good structural efficiency, and the biplane effect increasing forward flight efficiency relative to a single main rotor helicopter. Figure 22 depicts the Class A coaxial helicopter. The coaxial helicopter in this study has faired hubs and has been designed to stand fairly high, with no hangaring height constraint imposed. The lower rotor pitch links are exposed, and the upper rotor swashplate and pitch links are faired.

A high efficiency civil tiltrotor (HECTR) is a candidate vehicle for each of the size classes, and represents a higher-speed solution. Key features of the vehicle are related to its high cruise efficiency and its more moderate weight penalty than a traditional tiltrotor. The technologies and approach are in line with the High Efficiency Titlrotor (Ref. 19) and LCTR2. In addition to the usual advanced technology assumptions of composite materials and advanced drive system materials, the HECTR includes some design features which result in a fundamentally different solution than a conventional tiltrotor. The main design feature which drives a departure from conventional tiltrotors is the large reduction in rotor speed in cruise, which leads to different design approaches for other parts of the system, and the simultaneous application of these approaches takes the design away from the local optimum for the conventional tiltrotor. Because rotor speed varies so much, a very lightweight, stiff rotor is necessary, this alone reduces rotor weight. The low cruise rotor speed reduces the required stiffness for the wing to avoid whirl flutter, which can reduce weight and drag. The segregation of torque delivery from thrust and moment capacity turns the cowling into a load bearing structure, and lightens the transmission case. The wing extensions (portion of the wing outboard of the nacelle, which tilt with the nacelle) are not a requirement for the HECTR approach to work well, but when used, the extra thrust in hover (due mostly to added weight of extensions) must be offset by the gain in cruise efficiency. When wing extensions are not present, weight can be removed for both the extensions themselves and for the carry-through structure. The HECTR also has a two-speed transmission, which enables the large rotor speed variation within the bounds of operation of a turboshaft engine; this has a weight penalty with respect to a single-speed drive system, which must be offset by other system efficiencies. Fig. 23 depicts the Class A HECTR, which has no wing extensions and 3-bladed rotors. Fig. 27 depicts Class B HECTR which has wing extensions and 4-bladed rotors. Fig. 31 depicts Class C HECTR, with a large regional transport fuselage and wing extensions.

A side-by-side helicopter (SbS) is also a candidate vehicle which is considered. The side-by-side maintains a low disk loading, has a substantial improvement in cruise efficiency due to high effective span, and suffers less weight penalty than a tiltrotor.

Fig. 25 depicts the side-by-side helicopter for Class B.

The process by which the Class B side-by-side was designed is described in some detail within the Results section of this paper. The SbS design in this study forgoes the strut-braced approach of prior SbS aircraft, using instead a single support for the rotors. The support is modeled in NDARC as a tiltrotor wing, with strength sufficient for the 2g jump takeoff, and with stiffness for helicopter-mode stability but without high-speed whirl flutter actively sizing the wing. The wing of the SbS generates no lift, and has a fairing to reduce drag somewhat. A 40% thick wing section is modeled, with a constant drag coefficient of 0.0500, or about four times what a conventional tilt rotor wing might have. Refinement of the drag estimate and trade-offs with lifting wings were beyond the scope of this study.

A variation of the side-by-side, with 4 laterally displaced rotors (SbS4), was also considered (Fig. 26). While the effective span continues to grow, the interaction between adjacent rotors will sometimes involve the advancing blades, and sometimes the retreating blades.

OPTIMIZATION STRATEGIES

In order to efficiently explore the design space, a robust design (problem formulation and vehicle characteristics) must first be developed. In fact, several initial designs were selected as "seeds" for optimization, because of the complexity of the design space and the limitations of the current tools for supporting heuristic exploration of changeable vehicle topology. Each of these seed designs had a small degree of optimization by the designer, and were therefore expected to be located in the design space somewhat near a local optimum, or at least to have a value of the objective function close to that of a local optimum.

Each seed design was then optimized using a gradient-based optimization, in this case Sequential Least Squares Programming (SLSQP), one of the default optimizers in OpenMDAO. The derivative calculations for the optimizer were performed by finite-differencing of solutions. Neither the optimizer nor the finite-differencing method are ideal from a computational efficiency standpoint, but they have the advantage that the solver is quick to setup and finds optima with little effort or time. The optimization runs execute in tens of minutes on a desktop computer (Intel Core i5 or i7, 2.6GHz). A typical NDARC design run takes on the order of 10 seconds. Generating geometry with Alpine and OpenVSP takes about 10 seconds. The current implementation of the NDARC wrapper in RCOTools takes on the order of 10 seconds. Therefore, a single evaluation of a closed NDARC design may take on the order of a minute. The process of finding derivatives is amenable to parallel speedup, as the instances of the tools are independent of each other, but there is the potential of a bottleneck in the file system, as the communication between tools involves file input and output.

While the computational efficiency is a concern, the bigger concerns for a designer are the risk of missing a global optimum and the potential for NDARC to fail to converge (or diverge) due to poor initial conditions or inappropriate solution procedure parameters. Robustness of the solver is an area of ongoing research, in order to improve both gradient-based and gradient-free optimizations.

Emission Metrics and Objective Functions

Two emissions metrics have been selected: the Emissions Trading Scheme kg of CO_2, and the Average Temperature Response. These metrics are focused on the long-term climate change which comes about due to operation of the vehicles, and are, in absence of an excise tax or other mechanism, externalities to the operator of the vehicles. For the present study, each metric was used in isolation as an objective function, to examine how optimizing for one might unintentionally impact the other.

The ETS metric correlates directly with energy consumption in the mission, therefore, it behaves in the same way that the direct operating cost of fuel does. For this reason, achieving reductions in ETS is often a by-product of optimizing for minimum direct operating costs, especially in periods when cost of energy is expensive.

ATR has a more complicated interaction, as the Aviation Induced Cloudiness term dominates when active. In addition to the high magnitude ascribed to AIC, it has a high degree of uncertainty in its influence on global temperature. One factor which has not been included in our model for AIC influence on ATR is the time of day of the flight. Since the sizing missions have no diurnal factor, flights during daylight hours are treated the same as flights in darkness. Current models for the climate influence of AIC not only estimate different magnitudes to the effect based on day or night time cloud formation and dissipation, but the sign of the effect may also change. During the day, sunlight is absorbed and reflected away from Earth by AIC, reducing day time heating; at night, the radiation of heat from the Earth is reflected back downward, reducing night time cooling.

As a result of the indirect consequences and uncertainties, we have elected to report the results of emissions optimization without selecting one as preferable to another. The main results sought here are that design choices have measurable consequences for emission metrics, and that significant reductions might be achievable by using those design metrics.

Design Variables

The top-level design variables selected for this study were selected to represent those aspects which are likely to be within the designer's control.

Main rotor disk loading is often a design target, and is tightly correlated to hover performance, with an influence on cruise as well. Disk loading can significantly change the weight of the aircraft, which impacts energy consumption. Wing loading is similar to disk loading, except that it only applies to wing-borne aircraft and has a bigger effect on cruise performance. Hover download is slightly effected by wing

loading. Cruise efficiency and altitude capability are both effected by wing loading, especially for tiltrotors where the wingspan is largely pre-determined by rotor size and placement, and therefore wing loading corresponds to aspect ratio.

Main rotor tip speed in hover and cruise also have the potential to impact mission energy burn. For the tiltrotor, the cruise tip speed impacts not only cruise efficiency but also the required stiffness of the wing to maintain safe separation from whirl flutter.

From a mission standpoint, the cruise altitude is often a design variable for rotorcraft. While fixed wing jet transports tend to operate where assigned by air traffic control, and in the mid-30,000 ft altitudes, rotorcraft have a much wider altitude range to operate in while en route.

RESULTS

A common theme in the observed results is that the choice of vehicle type has a very large effect on the emissions, and optimization of design parameters at the vehicle level within a type generally has less of an influence. There is substantial opportunity for optimization of components, however, as the introduction of advanced technologies can fairly significantly reduce emissions, and this is really an indication of optimization in subsystems.

Results for Class A

Seed vehicles properties and results are tabulated in Table 3. For the Class A vehicles, changes to the type of aircraft and optimizing on high-level vehicle design parameters alone could not reduce the emissions to the 50% goal. Alternative propulsion schemes such as batteries and fuel cells were also unable to reduce the emissions for the design mission, because these aircraft were not capable of performing the design mission. The coaxial helicopter was the subject of excursions for batteries and fuel cells. An interesting observation is that the battery-powered aircraft generates 26% (ETS) to 30% (ATR) of the emissions produced by the turboshaft-powered coaxial helicopter, in order to go 25% of the range. The situation for the hydrogen fuel cell excursion is somewhat better, generating 18% (ETS) to 20% of the emissions of the coaxial turboshaft to go 25% of the range.

Considering Emissions Leads to Different Optima

Aircraft are often designed with a direct economic metric such as flyaway cost, mission fuel burn, or direct operating cost per available seat mile, as a major part of the objective function. Sometimes an indirect cost, such as scheduling timetables, or income from servicing a market via some signature capability, is used as part of the design objective function. These direct and indirect objectives lead designers to different places in the design space, and, as it turns out, the externalities associated with vehicle emissions can also drive the designs to different optima.

As an example, consider the HECTR aircraft for Class A, which is a very capable aircraft, but achieves this capability at a higher gross weight than some other options we have considered. In order to visualize some of the design space, a set of parametric sweeps have been run, varying disk loading and observing the resultant aircraft. Note that the geometric constraints of a tiltrotor result in wingspan increasing with radius, and if wing area is fixed, then aspect ratio increases. In actuality, the sizing relations are somewhat complicated when specifying disk loading and wing loading, as increases in radius, span, and aspect ratio may cause weight to grow dramatically, and thus a very nonlinear variation in radius with diskloading results.

Even this simple trade results in various aspects of the cost relationship finding very different optima; often at opposite ends of the trade space. In order to estimate costs, the relations within NDARC for flyaway cost (Harris-Scully CTM model) and maintenance cost (Harris model) are employed. Figure 4 shows that low disk loading (between 8 and 9 lb/ft^2) minimizes fuel burn, and high disk loading (still improving above 15 lb/ft^2) reduces block time. Fuel burn and block time are each elements which contribute to direct and indirect costs of operation. In terms of flyaway cost proxies, the CTM cost

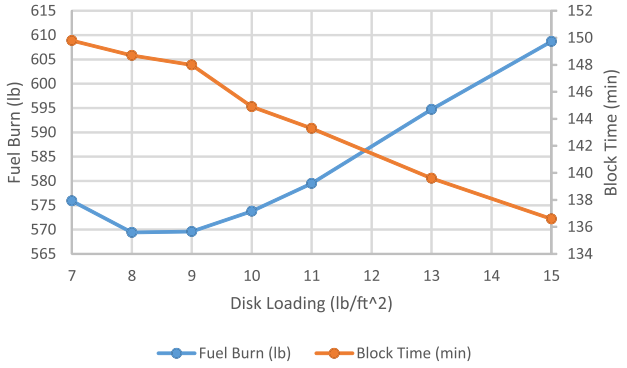

Fig. 4. Saving fuel costs results in increased block time for HECTR

model indicates a strong correlation between cost and vehicle empty weight and installed power. Figure 5 shows empty weight having a minimum above 15 lb/ft^2, and installed power having a minimum below 7 lb/ft^2. In order to reconcile the net effect of the divergent behavior of empty weight and installed power, it is a simple matter to calculate the CTM flyaway cost, which does indeed have a single-moded optimum behavior with respect to disk loading at around 9 lb/ft^2. However, Figure 6 shows how a focus on the flyaway cost might lock in years of higher maintenance cost for the fleet. It is unclear which of these two should dominate, as opportunity cost and finance costs must be considered in relation to the operation and support costs.

The pressurized HECTR is an interesting case study, however, as it provides opportunity and complication to our optimization. In Figure 7 we see that flying higher than 21,000 ft or so results in a strong divergence between the two metrics, with the Aviation Induced Cloudiness (AIC) component of

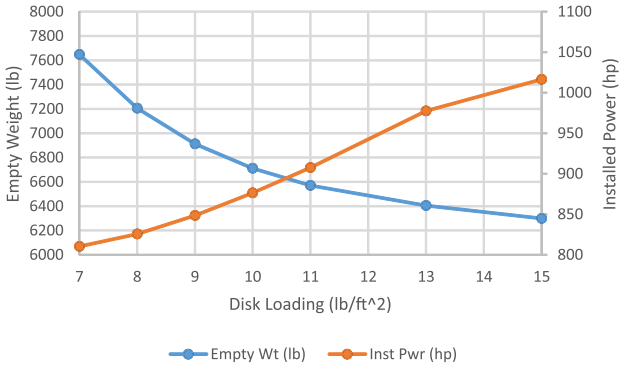

Fig. 5. Flyaway cost elements have divergent behavior for HECTR

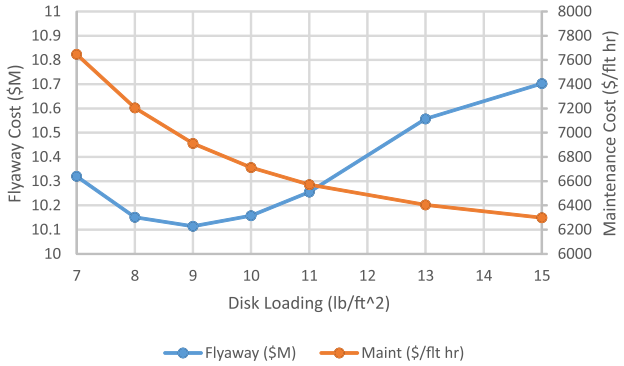

Fig. 6. Minimum flyaway cost increases maintenance cost for HECTR

ATR completely dominating. In addition, the ATR metric is multi-modal in this range of study, and a gradient-based optimization starting from low altitude might never climb past the mid-altitude rise to reach the minimum around 20,000 ft cruise altitude.

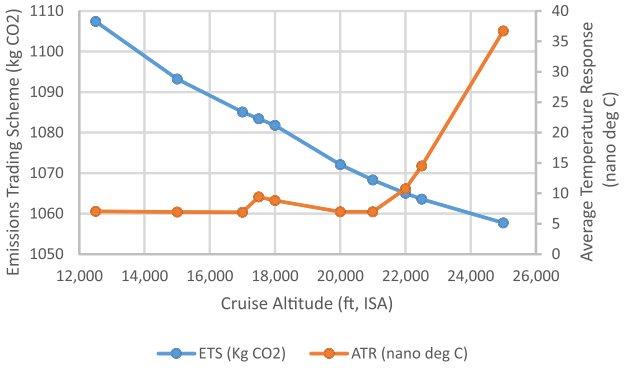

Fig. 7. Aviation induced cloudiness dominates high-altitude emissions for HECTR

For emissions, there is almost a direct correlation between mission fuel burn and the two emissions metrics. In Figure 8, we see how for a fixed cruise altitude, the two emissions metrics have essentially a constant scaling relative to each other over the range of disk loading considered, with a minimum near 8 lb/ft^2. Figure 4 indicates that fuel burn has its minimum between 8 and 9 lb/ft^2 as well. For all of the aircraft considered except the HECTR (which is able to fly quite high for cruise efficiency), this relationship holds, and one might be tempted to conclude that either ETS or ATR, or fuel burn for that matter, would be a good single metric for emissions of hydrocarbon-burning vehicles.

The HECTR result here is also instructive in that initial optimization had selected an aircraft without wing extensions, and for the ATR metric, it may also select an aircraft without pressurization as well (the pressurization weight penalty may offset the reduced fuel burn at altitude). For both removal of the wing extensions and conversion to an unpressurized aircraft, there are several values in the inputs which must be changed in a self-consistent way, and at present, there is no algorithmic method to perform these changes. At present, the designer is responsible for providing a self-consistent starting point for the optimizer to pursue. Further research and development will be required in order to develop robust algorithmic methods for changing topologies and aircraft types. For a HECTR in Class A, wing extensions do not result in enough of an improvement in performance to offset the increased weight and installed power. For a pressurized HECTR, flying as high as permitted by pressurization, up to about 25,000 ft, achieves lower ETS as the fuel burn is reduced. For a pressurized HECTR optimized to the ATR metric alone, flying at around 21,000 ft is a good solution. For an unpressurized HECTR, flying at the highest permissible altitude (12,000 ft) is optimal, as it reduces fuel burn and does not incur an AIC penalty.

Since it was not the purpose of this study to suggest the universally correct emissions metric, we simply identify these instances of conflicting objectives and topological complexity (both aircraft topology and solution space topology), as they provide good tests of the robustness of a design approach. The HECTR example thus provides a very good rationale for further study of methods to perform gradient-free optimization and guided design space exploration. More design space exploration and gradient-base/gradient-free optimization with the pressurized Class A HECTR is presented by Khurana (Ref. 20).

For the ATR metric, there is a strong influence of AIC, such that when it is present, it is the only important factor. Below approximately 22,000 ft altitude, little or no aviation induced cloudiness is formed, and the ETS and ATR metrics behave the same (Ref. 4). However, cruising above this altitude reduces ETS slightly and increases ATR significantly. To look at the design trades, an unpressurized HECTR is designed, cruising at 12,500 ft, without weight penalties for pressurized fuselage, doors, onboard oxygen generation, or pressurization systems. The pressurized aircraft compares similarly in terms of ETS, but is much worse in terms of ATR. This is a stark reminder that optimization metrics should be selected carefully, and that designer judgment is necessary to look at different solutions.

Results of running the gradient-based optimizer with two different starting points are shown in Fig. 9 and Fig. 10. The starting altitudes were selected on either end of the local minimum region for ATR with respect to altitude. There

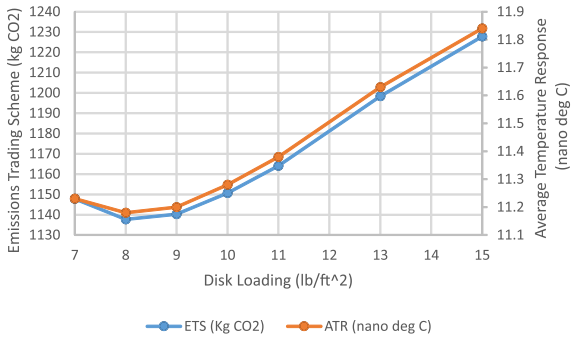

Fig. 8. Both ETS and ATR respond similarly to disk loading variation for HECTR

is clearly sensitivity to the design variables, as indicated by the big intermediate swings in the calculated objective value during the finite-difference checks, but the optimizer improves the initial value by approximately 2% in each case. The lower altitude case (Fig. 9) results in a solution about 2% better than the high altitude starting case. It is also interesting that the optimal disk loading and wing loading are different for the two cases. As a separate check of how the optimizer behaves

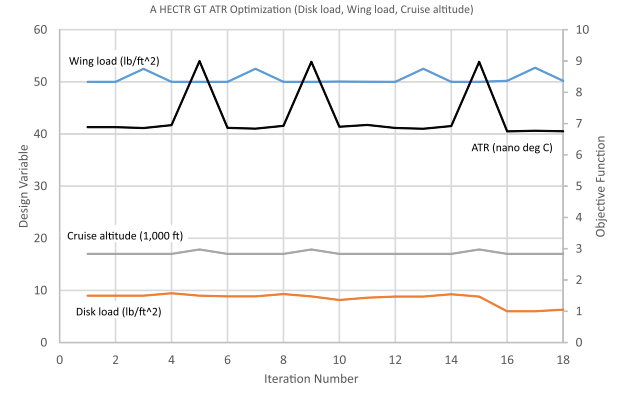

Fig. 9. Gradient-based optimization yields little improvement on the starting value for HECTR

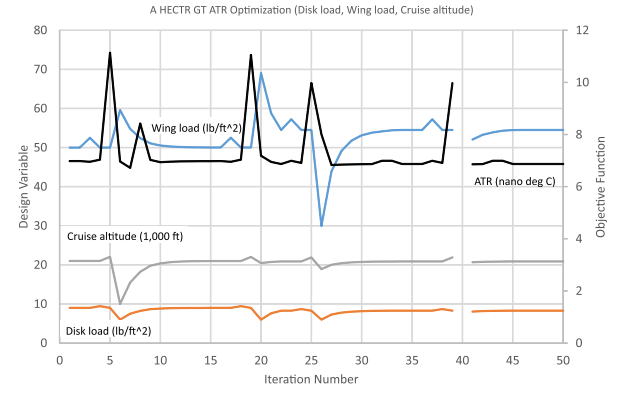

Fig. 10. Gradient-based optimization yields little improvement on the starting value for HECTR

when given a very different starting point, consider Fig. 11. The altitude stays low, but the disk loading goes fairly low and the wing loading somewhat high. The reduction in ETS from the starting point is 4.5%, and ATR follows along with it, reducing by 4.5% as well. The final value of ATR, however, is 17% worse than the final value shown in Fig. 9.

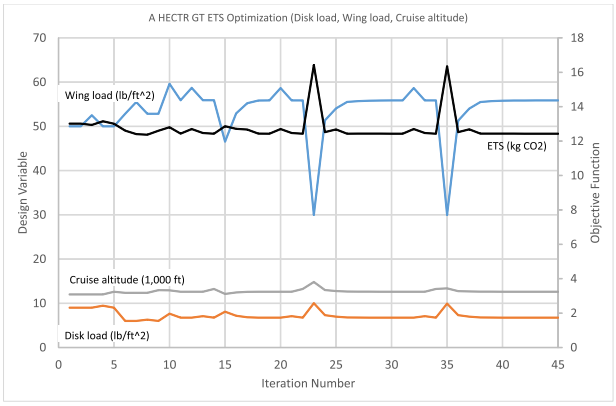

Fig. 11. Very different optimum found here for HECTR, due to a different starting point

Comparing the various vehicles, it is instructive to consider where power is being drawn and how much energy each segment consumes relative to the total. Fig. 12 shows that the takeoff power sizes the engines in both cases, and that the advanced technology aircraft requires significantly less power throughout. Fig. 13 shows that the coaxial helicopter requires

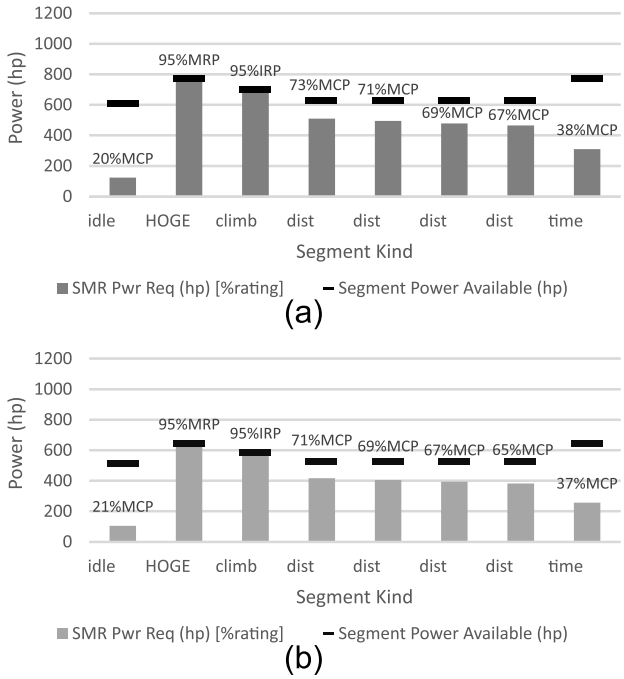

Fig. 12. SMR design mission segment power, (a) baseline, (b) advanced tech

less power in general than the baseline helicopter, and has a

quite efficient cruise. The hover sizing of the coaxial helicopter results in fairly low power installed (higher figure of merit), and therefore the best-range cruise power is closer to the continuous power limit. Battery and fuel cell variants each are sized larger, despite their shorter range. The battery and fuel cell aircraft have had their installed power sized by a speed sizing condition (150 KTAS, 90% MCP), and therefore the mission segments for hover and cruise have significant margins.

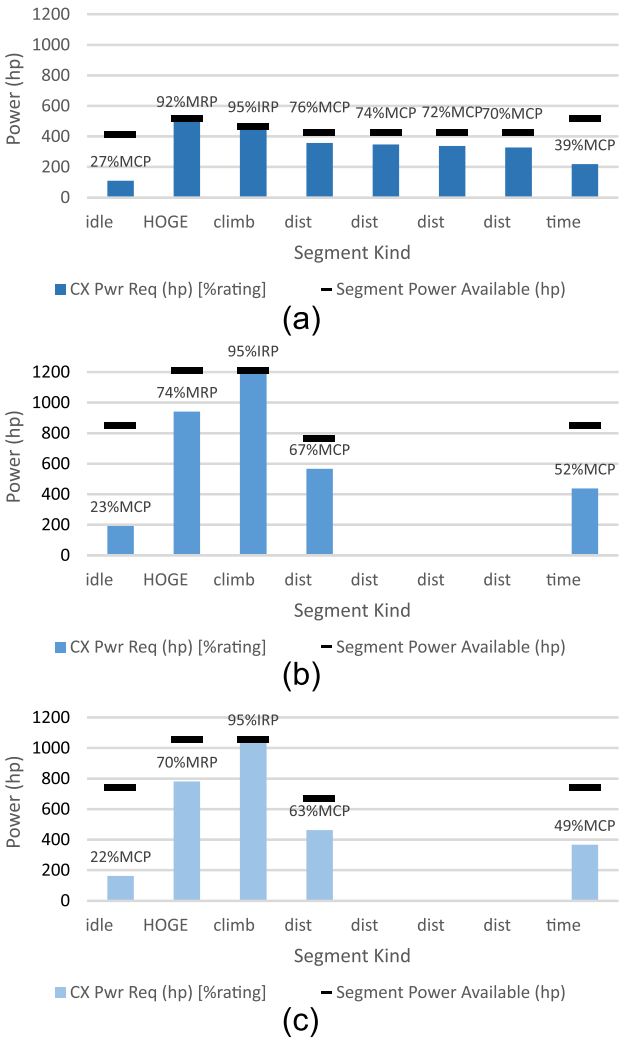

Fig. 13. Coaxial design mission segment power, (a) turboshaft, (b) Li-ion battery, and (c) hydrogen fuel cell

Fig. 14 shows the pressurized and unpressurized HECTR aircraft. Flying at 25,000 ft cruise altitude, the pressurized HECTR operates closer to its maximum continuous power limit (engine lapse with altitude). The increase in power required for the pressurized HECTR is offset by a higher cruise speed, so the total energy burn is less to go the same range.

These results lead us to the conclusion that blind adherence to a gradient-based optimization approach will likely lead us into a local optimum. The design space for this problem has discontinuities and is apparently quite multimodal. As

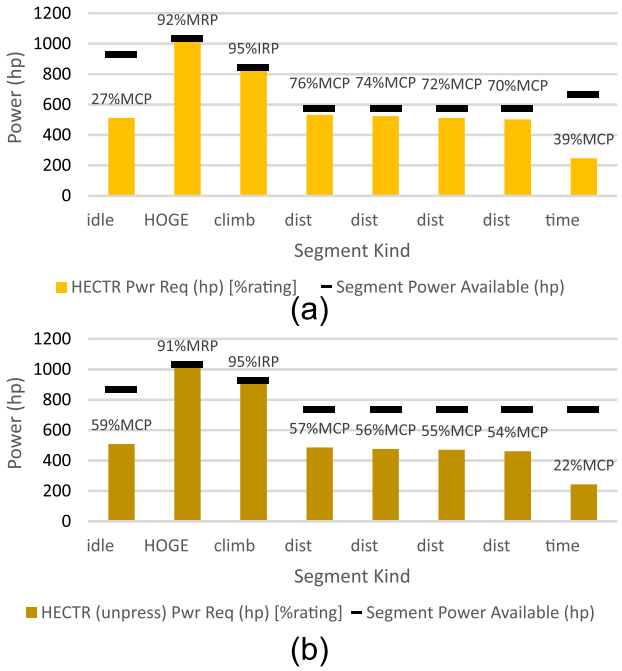

Fig. 14. HECTR design mission segment power, (a) Pressurized, (b) unpressurized

a result, future work should include conceptual design tools for design space exploration, rather than focusing on formal optimization.

Results for Class B

One possible way to improve the emissions of Class A vehicles is to design a new turboshaft engine, specifically seeking to reduce fuel consumption and emission products. Looking at Class B is instructive, as will be seen that the new turboshaft engine and other technologies nearly result in the advanced technology SMR meeting the 50% emission reduction target. The tabulated design information and performance results for the seed vehicles in Class B are shown in Table 4. For Class B, the HECTR seed aircraft has been designed to fly at 22,000 ft, and the ETS and AIC metrics both show reductions in excess of 50% with respect to the baseline aircraft. The larger payload and range of the design mission for Class B make the fuel burn in cruise a much bigger factor, which also contributes to the bias toward cruise-efficient aircraft. Gradient-based optimization of the Class B vehicles yields similar results to the A vehicles, as the design space is multimodal, and the seed vehicles are placed near local minima which are fairly close to the global optimum for the design variables and constraints.

Side-by-Side Design and Optimization

The Class B side-by-side helicopter is interesting as it and achieves greater than 50% reduction in emissions, and does so with a much lower installed power than the baseline SMR or the HECTR. Several publications have indicated a mutually

beneficial interaction for two rotors placed side-by-side with some overlap and intermeshing.

Mil (Ref. 21) has provided some early evidence of this phenomenon based on theory and testing, and Johnson (Ref. 22) discusses the theoretical boundary of performance. Tishchenko (Ref. 23) provides an anecdotal discussion of the benefits of the side-by-side type of aircraft in forward flight, with the example of the Mil V-12. In recent years, Korotkevitch (Ref. 24) and Silva (Ref. 25) each have discussed conceptual designs employing side-by-side rotor systems for cruise efficiency. These studies, however, do not provide a definitive guide as to the optimal spacing or rotor design for a vehicle system, accounting for airframe structure and drag.

The aircraft and rotor performance optimization was conducted as an iterative process using CAMRADII to calculate single and twin rotor performance, and NDARC to size the complete aircraft. The objective was to establish the design parameters for the best aircraft: particularly disk loading, blade twist, rotor separation (wing span), and tip speed. The primary objective metric for this optimization was fuel burned in the mission, as a driver of emissions. For the Class B SbS, the optimization involved the following steps, also presented in Table 5:

1) NDARC initial aircraft design
The initial aircraft designs were based on a baseline single-main-rotor performance model: σ=0.09, twist= 10^o/R, V_{tip}=700 ft/s, N_b=4, current technology airfoils; with blade tip swept, drooped, and tapered. The designs used default twin-rotor performance influence. The optimum (lowest weight) solution was disk loading=8 psf, span=35 ft=0.87D, cruise altitude=10,000 ft; R=20.2 ft, σ=.0949, V_{br}=133 knots.

2a) CAMRADII rotor suboptimization
Twin rotor performance was calculated for GW=20,000 lb, R=20 ft; σ=0.0949, 4 blades, articulated, current technology airfoils; tip sweep (15 deg) and taper (60%) at 0.94R. The wake model was based on tandem helicopter models. Tip vortex core=0.4*chord (default 0.2*chord) helps obtain smooth trends. For twist and span optimization: twist= 6 to 21 ^{o}/R; span=0.75, 0.875, 0.90, 0.925, 0.95, 1.00D.
i) Span=0.925D has lowest cruise power, any twist.
ii) Span=0.75D has lowest hover power, any twist (span effect less than twist effect).
iii) Optimum (lowest power) twist = 11 ^{o}/R for cruise, 21 ^{o}/R (at least) for hover.
iii) Optimum (lowest power) twist = 11 ^{o}/R for cruise, 21 ^{o}/R (at least) for hover.
iv) Calculate power and C_{do} for NDARC, for span=0.875D, twist= 11 to 21 ^{o}/R, forward flight (133 kt) and hover.

2b) NDARC design suboptimization
For off-design conditions of GW=20,000 lb, hover and forward flight (133 kt); set C_{do} to CAMRADII value and adjust Ki to match CAMRADII power. Then size aircraft, find fuel flow for design mission (fly at 133 kt). For span=0.875D, minimum fuel burn occurs for twist= 16^o/R; σ=0.0949, V_{br}=182 knots.

3a) CAMRADII rotor suboptimization
V_{tip}=700 ft/s and V=182 ktas gives M_{at}=0.934. Reduce tip speed to reduce advancing tip Mach: V_{tip}=650, V=182 gives M_{at}=0.887. With increased chord (σ=0.110), more induced power and less profile power for all twist, total power about the same. For twist and span optimization: twist= 6 to 21 ^{o}/R; span=0.75, 0.875, 0.90, 0.925, 0.95, 1.00D.
i) Span=0.90D has lowest cruise power, any twist.
ii) Span=0.75D has lowest hover power, any twist (span effect less than twist effect).
iii) Optimum (lowest power) twist = 13 ^{o}/R for cruise, 21 ^{o}/R (at least) for hover.

3b) NDARC off-design rotor model check and find flight speed
For off design conditions of GW=20,000 lb, hover and forward flight (133 kt); set C_{do} to CAMRADII value and adjust K_i to match CAMRADII power. Then size aircraft, find fuel flow for design mission. Fly mission at 170 and 160 knots, span=0.90D, twist= 13 ^{o}/R: 160 knots has lower GW, power, fuel burn.

3c) CAMRADII rotor suboptimization
Span=0.90D, twist=12 to 21 ^{o}/R, forward flight (160 kt) and hover.

3d) NDARC design suboptimization
Lowest fuel burn for 160 knots, span=0.90D, twist= 17 ^{o}/R.

3e) CAMRADII rotor suboptimization, introduce bilinear twist
Optimize bilinear twist for span=1.80D, hover and 160 knots: inboard twist and outboard twist = 20, 18, 16, 14, 12 ^{o}/R.
i) For hover: inboard/outboard twist <20 ^{o}/R best
ii) For forward flight: inboard/outboard twist = 16 ^{o}/R best.

4a) NDARC rotor model calibration check
NDARC single rotor performance calibration. Then NDARC side-by-side rotor performance calibration, for span=0.75, 0.80, 0.85, 0.90, 0.95, 1.00, 1.05D: matched total, induced, and profile power of CAMRADII twin rotor.

4b) NDARC design suboptimization
Optimize aircraft:
i) Disk loading=8 psf: best fuel burn for span=0.85D.
ii) Span=0.85D, relative disk loading=6 psf: disk loading=7 minimum GW (0.6%), 5.5 psf minimum power (2.6%), 5 psf minimum fuel burn (0.7%).
iii) Disk loading=6 psf: best fuel burn for span=0.85D.
iv) Disk loading=6 psf, span=0.85D: best fuel burn for 4 blades.
v) Disk loading=6 psf, span=0.85D: best fuel burn for tip speed 675 ft/s (σ=0.0766).

4c) CAMRADII
NDARC single rotor performance calibration for R=24 ft, σ=0.0766, V_{tip}=675 ft/s. NDARC side-by-side rotor performance calibration for span=0.85D.

5) NDARC design with optimized rotor system.
Aircraft relative baseline design: GW 70%, power 49%, fuel burn 53%. Aircraft relative baseline design with weight/engine/drag technology: GW 88%, power 59%, fuel burn 65%.

Fig. 15 shows CAMRADII twin rotor performance (L/De=WV/(P_i+P_o)) for span=0.75, 0.80, 0.85, 0.90, 0.95, 1.00, 1.05D (σ=.0766, V_{tip}=675, C_T/σ=0.098): best performance for overlap 10-15%, 15% optimum for aircraft (less wing weight and drag). Overlapped side-by-side rotor performance is about 20% better than separate, non-overlapped twin rotors. Wrong direction of rotation (retreating side outboard) is only a little better than separate rotors. Figures 16 and 17 show combined rotor wakes in forward flight, behaving like wake of single, larger span wing.

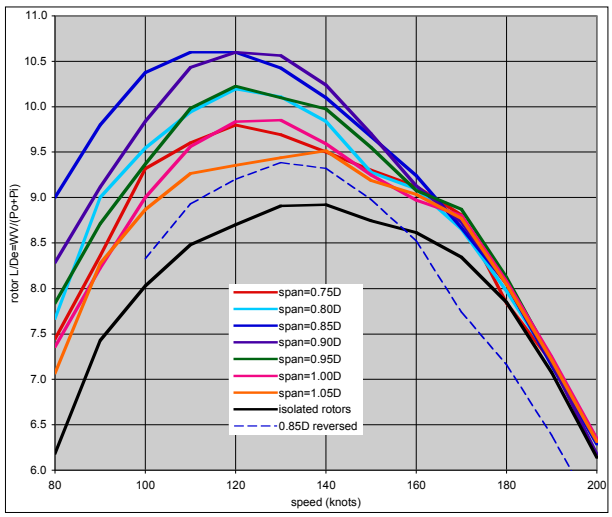

Fig. 15. Twin rotor free wake performance calculations of L/De=WV/(P_o+P_i) illustrate that outboard-advancing and 0.85-0.90D spacing is best

Fig. 18 compares the cruise efficiency of the SbS with that of some existing helicopters. As can be seen from the figure, the cruise efficiency is quite a bit higher than the existing aircraft to which it is being compared, and this is true over a wide speed range.

The question of how to integrate flyaway and maintenance costs, in addition to the objective of low emissions, is bought back to the fore when looking at the SbS. Without proposing a method for quantitatively factoring these into the design selection process, it is interesting to note that the SbS has a flyaway cost 32% below that of the advanced technology SMR and 50% below that of the HECTR. Fuel burn is 38% lower than the SMR and 24% higher than the HECTR. Further consideration of the SbS seems warranted, especially if direct costs and externalities are to be considered in future designs.

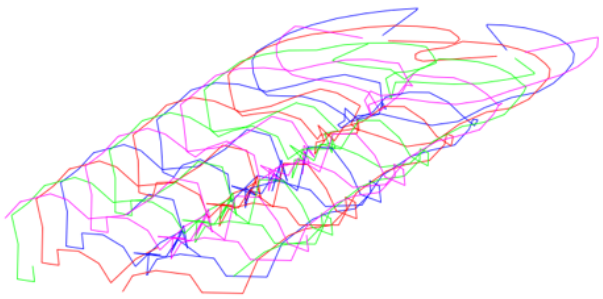

Fig. 16. Outboard blades advancing results in wake roll up with two large super-vortices outboard and a weak interaction inboard. Spacing=0.85D, μ=0.35

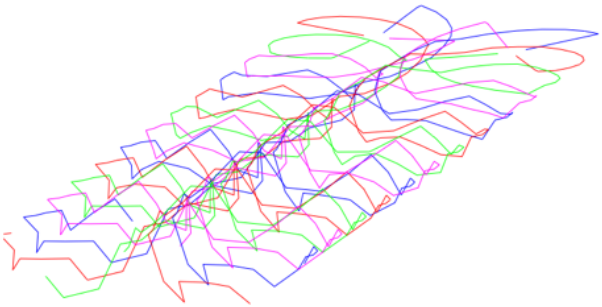

Fig. 17. Outboard blades retreating results in wake roll up with two large super-vortices outboard and a strong interaction inboard. Spacing=0.85D, μ=0.35

Excursions for battery electric and turboelectric vehicles have been performed, and the results are not unexpected. The battery results are similar to Class A, however with little hope that a SbS could achieve a reduction in emissions relative to a turboshaft based on current U.S. grid emissions. The turboelectric with battery design admittedly has not had much optimization and could use more research. However, a problem arises in that the turboshaft engine size is already fairly small, and reducing the engine size by using a battery assist in takeoff would likely increase the baseline specific fuel consumption of the turboshaft, as smaller engines tend to be less efficient. A smaller turboshaft would likely fall into the class of turboshafts used for Class A, and as discussed, this means giving up on technology which has been developed for larger turboshafts. Thus, gains in efficiency in cruise due to running at higher part power will be offset by losses due to having a smaller engine.

There is also some question regarding the practicality of side-by-side rotor systems. The CAMRADII analysis suggests that aerodynamics of side-by-side rotors will be characterized by unsteadiness and asymmetry. The wake interaction in the overlap region leads to unsteadiness in the flow, significant blade-vortex interaction with increased noise and vibration likely. Calculations also exhibit erratic behavior of

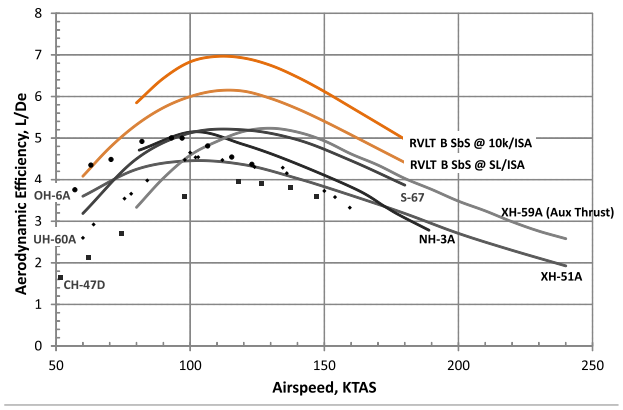

Fig. 18. Comparison of predicted cruise performance of Class B side-by-side with flight test data of several helicopters and compounds

performance, and the calculated wake tends to not be laterally-symmetric. The publicly available records of the Soviet-era experiences of Mil with side-by-side rotors are vague at best with regard to the instability of the wake and its implications for vehicle stability. At a minimum, this means that experimental data needs to be gathered for side-by-side rotor systems in order to (1) confirm the performance payoff, and (2) explore the instability of the wake.

The 4-abreast side-by-side helicopter (SbS4) also achieves the target for emission reductions. An excursion with slightly higher disk loading was performed, which indicates that the price of the extra span is offset by the increased drag of the support wing. The increased flyaway cost relative to the SbS makes it unlikely that the SbS4 would be selected instead, but it does still compare favorably to the SMR and HECTR.

Results for Class C

Class C results follow in line with Class A and Class B. The big difference is that the reduced emissions are achieved relative to a baseline aircraft which is already fairly efficient. This reduction is enabled by the long cruise of 1300 nm, which allows the cruise efficiency of the HECTR to reduce the fuel load substantially, which in turn reduces vehicle weight and thus the installed power.

SUMMARY AND FUTURE WORK

Software tools have been developed to flexibly and rapidly link various analysis methods to design advanced VTOL aircraft. At this time, automation has been introduced to quickly find local optimum designs, starting from a predefined self-consistent design as a starting point. Optimization for the externalities of emissions leads to different designs than optimizing on direct and indirect economics. Several reference vehicle types have been designed, with flexible inputs which may be extended by users of this tool set. The goals for 50% emissions reductions have been met for Classes B and C, but Class A has not met these goals, due to the dearth of fuel efficient engines in the 700-1000 shp size class. Results for the HECTR type of aircraft are representative, and are summarized in Table 2.

Table 2. Emission Reductions Achieved with HECTR

Metric	Class A	Class B	Class C
ETS	36%	69%	71%
ATR	34%	67%	72%

Future work integrating propulsion modeling will be performed to work toward the emission reduction targets, with the goal of applying advanced technologies and low-emission design criteria to achieve our target emissions. In particular, design of low-emissions engines in the range of 1,000 shp and below, should have a big impact on the ability to meet emission goals. The RCOTOOLS software package, the seed aircraft models, optimization problems, and results described herein will be made publicly available to researchers.

NOTATION

AIC	Aviation induced cloudiness
ATR	Average temperature response
b	Span (spacing between rotors for SbS)
Batt	(Lithium-ion) battery
CTM	Harris-Scully flyaway cost model
CX	Coaxial helicopter
D	Diameter
DGW	Design gross weight
ETS	Emission Trading Scheme
FC	(Hydrogen) fuel cell
HECTR	High efficiency civil tiltrotor
ktas	Knots true airspeed
n_b	Number of blades on a rotor
psf	Pounds (force) per square foot
R	Radius
SbS	Side-by-side helicopter
SbS4	Side-by-side with 4 rotors laterally
SLSQP	Sequential least squares programming
SMR	Single main rotor helicopter
TR	Tiltrotor
V_{br}	Best-range cruise speed (often taken as V_{LRC})
V_{LRC}	Long-range cruise speed, 99% high-side
WE	Empty weight
μ	Advance ratio
σ	(Thrust-weighted) solidity

REFERENCES

[1]Johnson, W. R., "NDARC NASA Design and Analysis of Rotorcraft," NASA/TP-2015-218751, November 2015.

[2]Moore, K. T., Naylor, B. A., and Gray, J. S., "The development of an open-source framework for multidisciplinary analysis and optimization," 10th aiaa/issmo multidisciplinary analysis and optimization conference, 2008.

[3]NASA, "NASA Aeronautics Strategic Implementation Plan 2017 Update," retrieved from https://www.nasa.gov/sites/default/files/atoms/files/sip-2017-03-23-17-high.pdf on 10 July 2017, 2017.

[4]Russell, C. and Johnson, W., "Application of climate Impact Metrics to Civil Tiltrotor Design," 51st AIAA Aerospace Sciences Meeting including the New Horizons Forum and Aerospace Exposition, 2013.

[5]Sinsay, J., Hadka, D., and Lego, S., "An Integrated Design Environment for NDARC," AHS Technical Meeting on Aeromechanics for Vertical Lift, 2016.

[6]Johnson, W. R., "CAMRAD II, Comprehensive Analytical Model of Rotorcraft Aerodynamics and Dynamics Manuals," Johnson Aeronautics, 2017.

[7]Hahn, A., "Vehicle Sketch Pad: Parametric Geometry for Conceptual Aircraft Design," AIAA 2010-657, 2010.

[8]Perry, T. D., "ALPINE: Automated Layout with a Python Integrated NDARC Environment," OpenVSP Workshop 2016, retrieved from: https://nari.arc.nasa.gov/sites/default/files/attachments/34ALPINE2017, 2016.

[9]Meyn, L. L., "Rotorcraft Optimization Tools: Incorporating Design Codes into Multi-Disciplinary Design, Analysis and Optimization," AHS Specialists Meeting on Aeromechanics Design for Transformative Vertical Lift, 2018.

[10]Lawrence, B., Theodore, C. R., Berger, T., and Johnson, W., "Handling Qualities Optimization for Rotorcraft Conceptual Design," Rotorcraft Virtual Engineering Conference, 2016.

[11]Rohl, P. K., Cesnik, C. E., Dorman, P., and Kumar, D., "IXGEN: A Modeling Tool for the Preliminary Design of Composite Rotor Blades," AHS Future Vertical Lift Aircraft Design Conference, 2012.

[12]Acree, C. W., Yeo, H., and Sinsay, J. D., "Performance Optimization of the NASA Large Civil Tiltrotor," NASA TM2008-215359, 2008.

[13]NASA, "Technology Readiness Level Definitions," retrieved from https://www.nasa.gov/pdf/458490main_TRL_Definitions.pdf on 28 Dec 2017.

[14]Chase, N., "JMR TD: Addressing the Needs of the Future Rotorcraft Fleet," AHS Aeromechanics Specialists' Conference, 2014.

[15]U.S. Department of Energy Fuel Cell Technologies Office, "Hydrogen Production: Natural Gas Reforming," Retrieved from https://energy.gov/eere/fuelcells/hydrogen-production-natural-gas-reforming on 23 Dec 2017.

[16]Bonaquist, D., "Analysis of CO2 Emissions, Reductions, and Capture for Large-Scale Hydrogen Production Plants," PRAXAIR white paper, 2010.

[17]Chavez, A., Baker, T., and Fetty, J., "Future Advanced Rotorcraft Drive System (FARDS) Full Scale Gearbox Demonstration," AHS International 73rd Annual Forum, May 2017.

[18]Berger, T., "Karem TR36XP DARPA VTOL X-Plane," AHS International 72nd Annual Forum, 2016.

[19]Silva, C., Calvert, M. E., Gallaher, A. T., Nunez, G. F., Scott, R. C., Sinsay, J. D., and Vocke, R. D., "The High Efficiency Tiltrotor as a Solution to the Needs of a Mobile Military," AHS Technical Meeting on Aeromechanics for Vertical Lift, 2016.

[20]Khurana, M. S. and Silva, C., "Optimization of a High Efficiency Civil Tiltrotor platform for Low Emission Flight," AHS Specialists Meeting on Aeromechanics Design for Transformative Vertical Lift, 2018.

[21]Mil, M. L., "Helicopters: Calculation and Design, Volume I," NASA TTF-494, 1967.

[22]Johnson, W., "Rotorcraft Aeromechanics," New York: Cambridge University Press, 2013.

[23]Tishchenko, M. N., "Mil Design Bureau Heavy-Lift Helicopters," journal of the American Helicopter Society, Vol. 42, Number 2, 1997.

[24]Korotkevich, M., Midzyanovskiy, S., and Ivchin, V., "Highspeed Rotorcraft of the MI-450 Family New Generation of Cross-Arrangement Rotary-Wing Aircraft," 40th European Rotorcraft Forum, 2014.

[25]Silva, C., "Conceptual Design of a Remote Controlled Electric Powered Helicopter for World Record Distance, Endurance, and Climb," AHS Technical Meeting on Aeromechanics for Vertical Lift, 2016.

Table 3. Class A Seed Vehicles

Aircraft	ID	A Baseline	A Tech	A Coax	A Coax bat	A Coax FC	A HECTR	A HECTR (unpress)	A Side
Type	ID	SMR	SMR	Coax	Coax	Coax	HECTR	HECTR (unpress)	SbS
Energy	ID	Jet A	Jet A	Jet A	Li-Ion	compressed H2	Jet A	Jet A	Jet A
Drive	ID	Turbo+ GB	Turbo+ GB	Turbo+ GB	motor+ GB	motor+ GB	Turbo+ GB	Turbo+ GB	Turbo+ GB
Disk loading[a]	psf	8.0	8.0	8.0	8.0	8.0	9.0	9.0	7.0
Wing loading [a]	psf	–	–	–	–	–	50	50	–
Hover V_{tip} [a]	ft/s	700	700	700	700	700	750	750	650
Cruise V_{tip} [a]	ft/s	700	700	700	700	700	383	383	650
Cruise altitude[a]	ft	9000	9000	9000	9000	9000	25000	12000	9000
DGW	lb	5781	4781	4586	8560	7027	7555	7505	4602
WE	lb	3597	2781	2694	7340	5749	5703	5621	2742
Installed power	hp	1070	970	766	1270	1104	1595	1495	720
CTM flyaway	$M	4.3	3.8	3.4	5.6	4.9	8.6	8.3	3.7
Design payload	lb	1000	1000	1000	1000	1000	1000	1000	1000
Design range	nm	400	400	400	100	100	400	400	400
Design takeoff energy	MJ	18692	15130	13030	2126	3203	12281	12865	12411
Fuel burn	lb	855	688	594	0	42	546	580	568
Cruise speed	KTAS	131	136	136	131	126	203	170	126
Emiss Trading Scheme	kg CO_2	1637	1325	1141	298	204	1076	1127	1087
Avg Temp Response	nano ^oC	10.4	8.4	7.3	2.2	1.5	36.8	7.2	6.9
ETS vs. baseline	% of base	0%	-19%	-30%	-82%	-88%	-34%	-31%	-34%
ATR vs. baseline	% of base	0%	-19%	-30%	-79%	-86%	+254%	-31%	-33%

[a]Possible design variables

Table 4. Class B Seed Vehicles

Aircraft	ID	B Baseline	B Tech	B Side	B Side E	B Side TE	B Side TEb	B Side 4	B Side 4 DL8	B HECTR
Type	ID	SMR	SMR	Side by Side	Side by Side	Side by Side	Side by Side	SbS (4)	SbS (4)	HECTR
Energy	ID	Jet A	Jet A	Jet A	Li-Ion	Jet A	Jet A+Li-Ion	Jet A	Jet A	Jet A
Drive	ID	Turbo+ GB	Turbo+ GB	Turbo+ GB	motor+ GB	motor+ GB	motor+ GB	Turbo+ GB	Turbo+ GB	Turbo+ GB
Disk loading[a]	psf	9.0	9.0	6.0	6.0	6.0	6.0	6.0	8.0	11.0
Wing loading [a]	psf	–	–	–	–	–	–	–	–	70
Hover V_{tip}[a]	ft/s	700	700	675	675	675	675	675	675	750
Cruise V_{tip}[a]	ft/s	700	700	675	675	675	675	675	675	383
Cruise altitude[a]	ft	10000	8000	10000	10000	10000	10000	10000	10000	22000
DGW	lb	36402	23638	20223	38598	21806	21646	21081	20636	26789
WE	lb	23942	13935	11906	32540	13134	13041	12272	12182	18304
Installed power	hp	9829	6765	3300	4678	3068	3063	3759	3822	7717
CTM flyaway	$M	37	25	19	33	34	33	22	22	39
Design payload	lb	5280	5280	5280	5280	5280	5280	5280	5280	5280
Design range	nm	500	500	500	100	500	500	500	500	500
Design takeoff energy	MJ	124426	70678	43780	8558	50807	49497	53310	46427	37982
Fuel burn	lb	5732	3243	2021	0	2347	2290	2474	2140	1625
Cruise speed	KTAS	141	143	138	123	139	138	133	140	213
Emiss Trading Scheme	kg CO_2	10897	6192	3835	1198	4409	4295	4670	4068	3326
Avg Temp Response	nano ^oC	68	39	24	9	28	27	30	26	27
ETS vs. baseline	% of base	0%	-43%	-65%	-89%	-60%	-61%	-57%	-63%	-69%
ATR vs. baseline	% of base	0%	-42%	-64%	-87%	-59%	-60%	-56%	-62%	-61%

[a]Possible design variables

Table 5. Initial Optimization of Class B SbS

	Initial State									Suboptimization result						
Code	σ	twist	V_{br}	v_{tip}	n_b	Disk load	b/D	R	GW	V_{br}	V_{tip}	σ	Disk load	b/D	twist hov / cr	R
ID[a]	-	^{o}/R	ktas	ft/s	-	psf		ft	lb	ktas	ft/s	-	psf	-	^{o}/R	ft
N	0.09	-10		700	4				20000	133		0.095	8	0.87		20.2
CII	0.095							20	20000					0.75 / 0.93	-21 / -11	
N		-16					0.88		20000	182				0.88		
CII		-6 to -21	182	700, 650			0.75 to 1		20000		650	0.11		0.75 / 0.90	-21 / -13	
N		-13	160, 170						20000	160						
CII		-12 to -21	160				0.9		20000	160				0.9	-17	
N																
CII		-12 to -20					1.8		20000						-20 / -16	
N							0.75 to 1.05		20000							
N						6 to 8	0.85		20000		675	0.077	6	0.85		24
CII	0.077			675			0.85	24	20000							
N	0.077	-16	160	675	4	6	0.85	23.2	20223							

[a]N = NDARC, CII = CAMRAD II

Table 6. Class C Seed Vehicles

Type	ID	TR	TR (tech)	HECTR
Energy	ID	Jet A	Jet A	Jet A
Drive	ID	Turbo+GB	Turbo+GB	Turbo+GB
Disk loading[a]	psf	20.0	20.0	15.7
Wing loading [a]	psf	120	120	74
Hover V_{tip}[a]	ft/s	792	792	750
Cruise V_{tip}[a]	ft/s	664	664	404
Cruise altitude[a]	ft	20000	20000	18000
DGW	lb	135260	91660	69163
WE	lb	90248	56097	40729
Installed power	hp	31586	21741	23722
CTM flyaway	$M	129	88	106
Design payload	lb	16500	16500	16720
Design range	nm	1300	1300	1300
Design takeoff energy	MJ	527583	344149	185919
Fuel burn	lb	25763	16821	8880
Cruise speed	KTAS	297	207	209
Emiss Trading Scheme	kg CO_2	46222	30151	16287
Avg Temp Response	nano ^{o}C	314	201	110
ETS vs. baseline	% of base	0%	-35%	-65%
ATR vs. baseline	% of base	0%	-36%	-65%

[a]Possible design variables

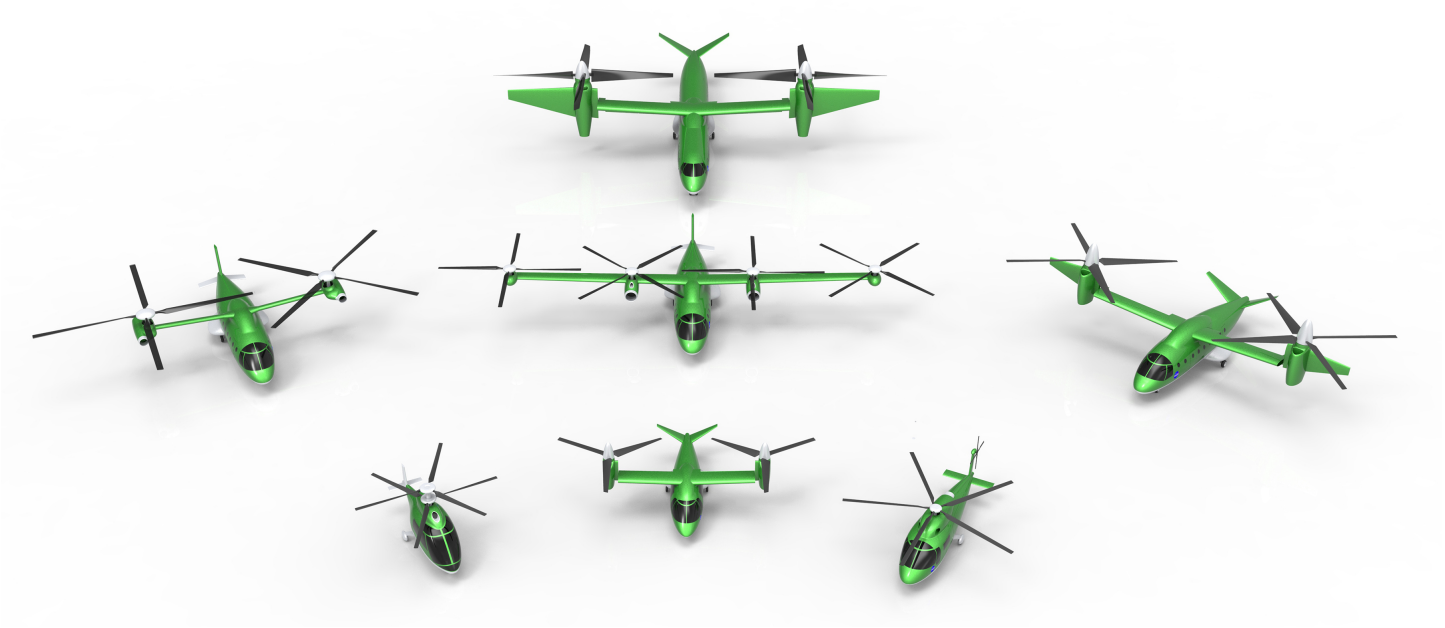

Fig. 19. Perspective rendering of various low-emission aircraft, illustrating the array of sizes and types in this study

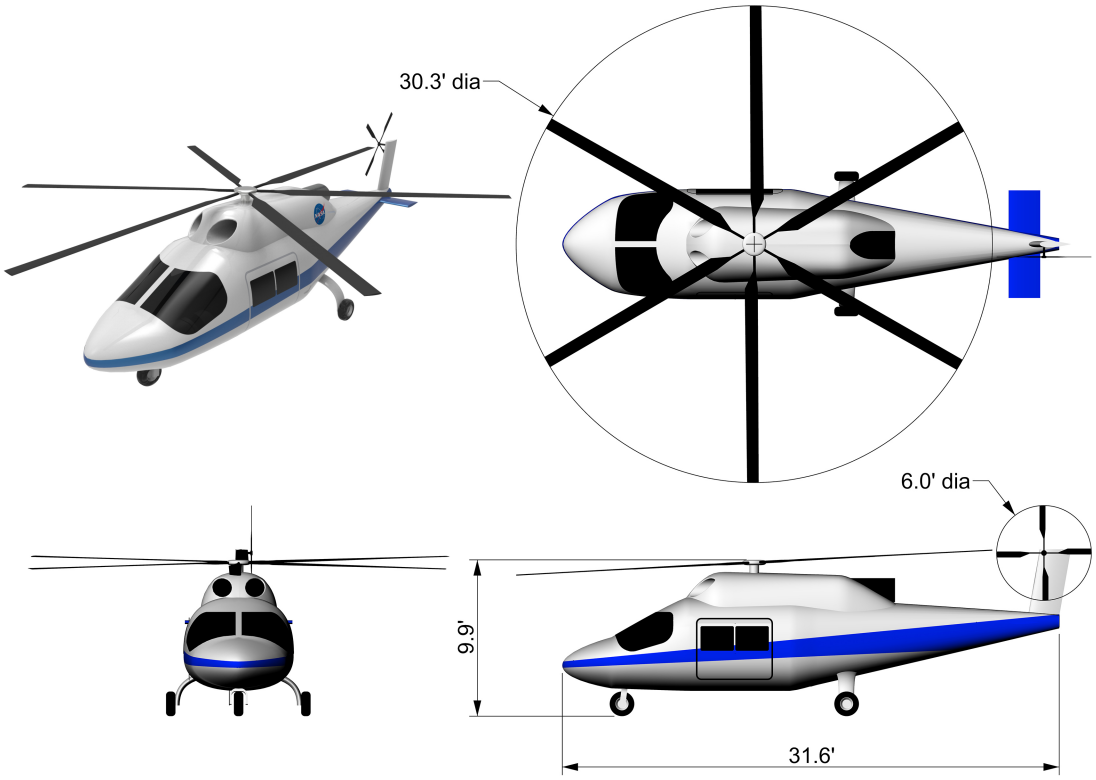

Fig. 20. Vehicle A Single Main Rotor Baseline

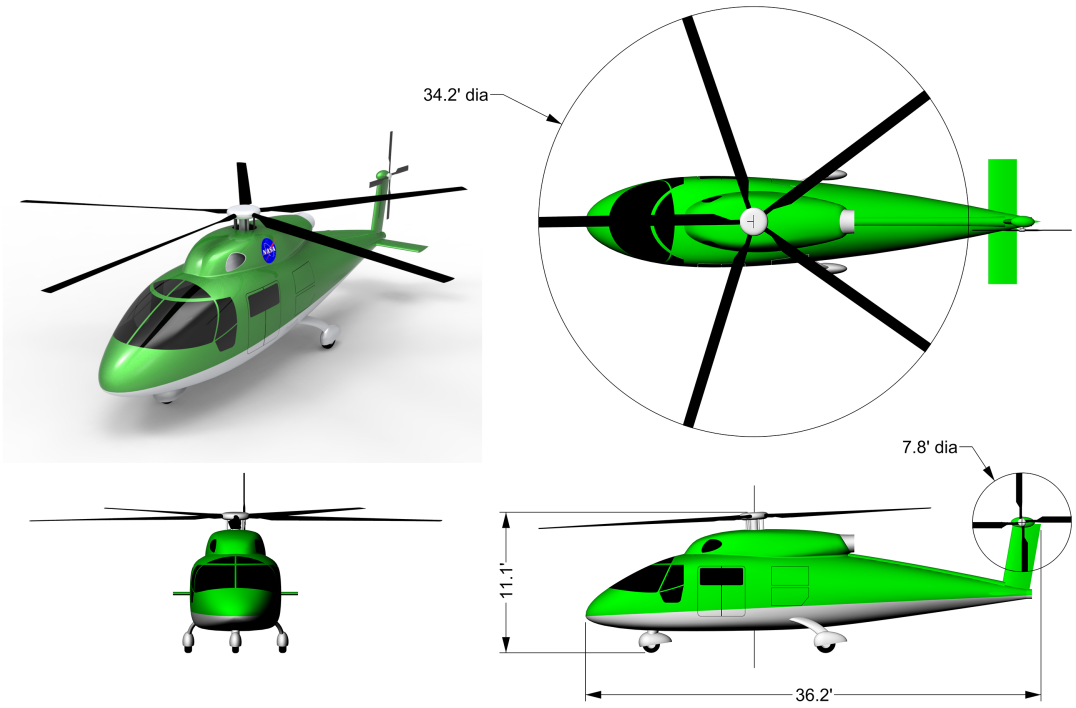

Fig. 21. Vehicle A Single Main Rotor Turboshaft

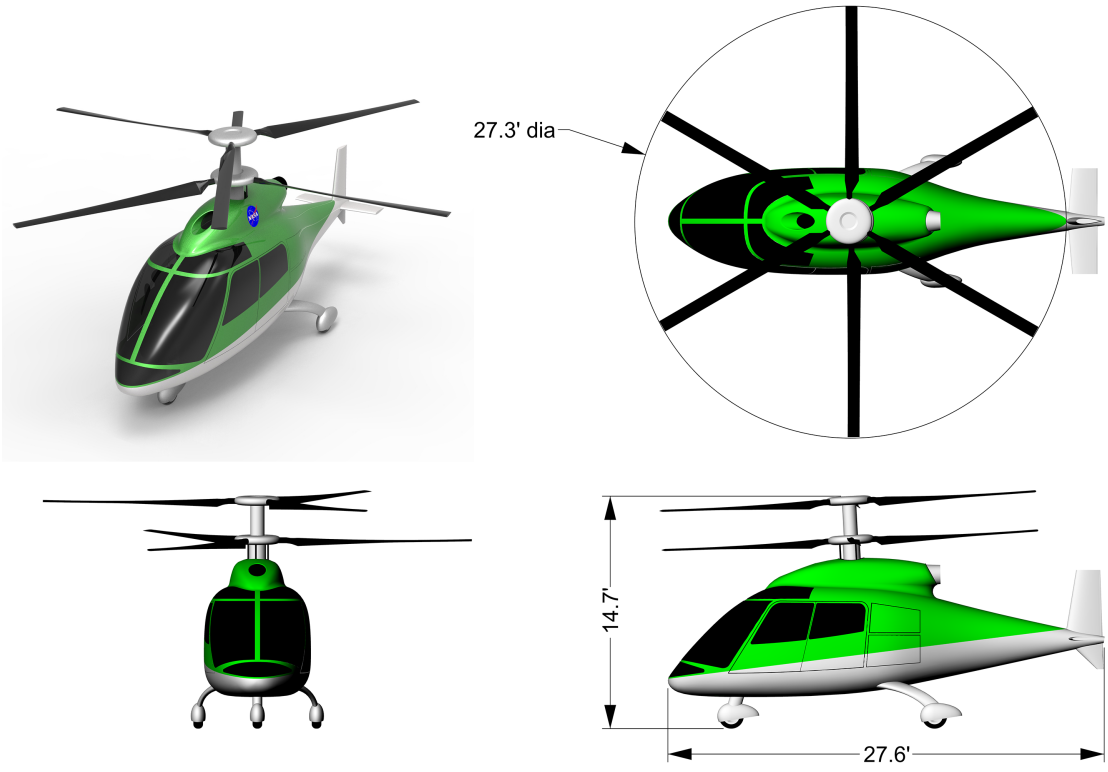

Fig. 22. Vehicle A Coaxial Turboshaft

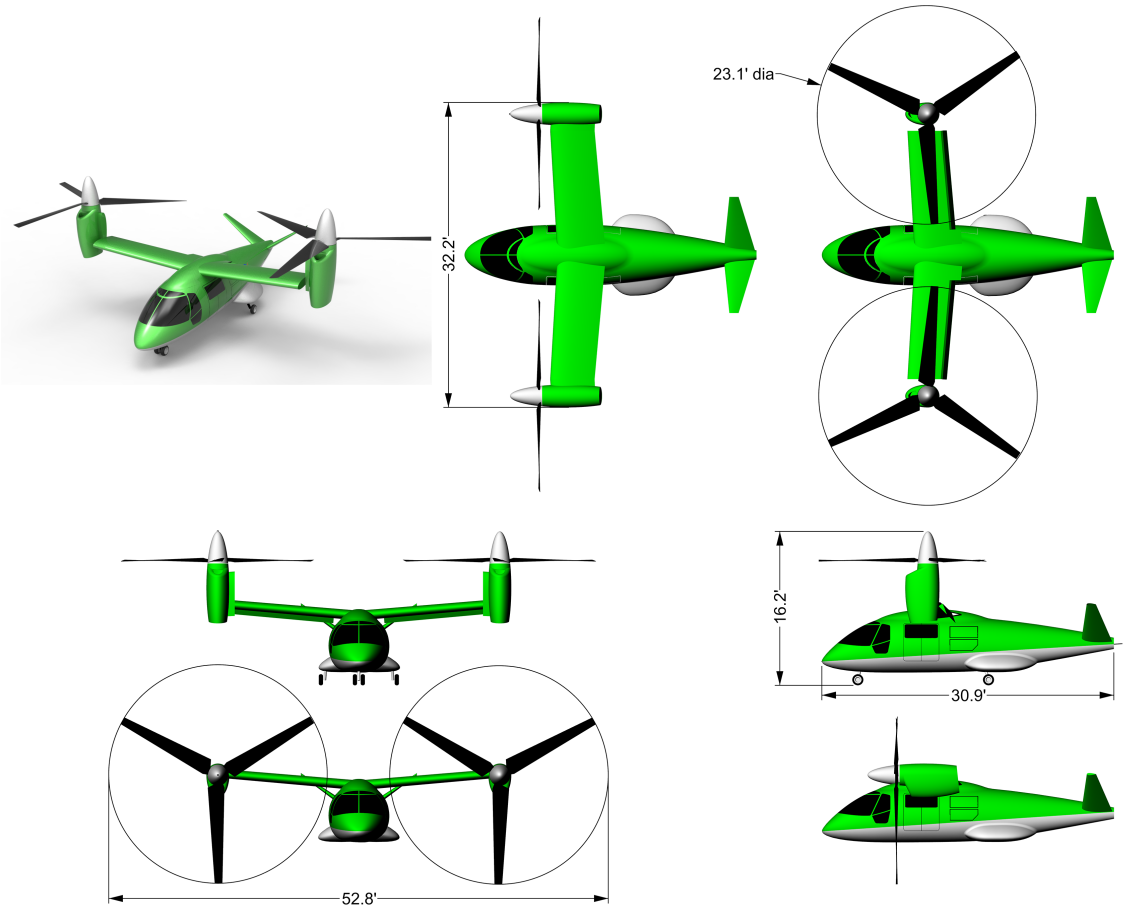

Fig. 23. Vehicle A High Efficiency Civil Tiltrotor (Turboshaft)

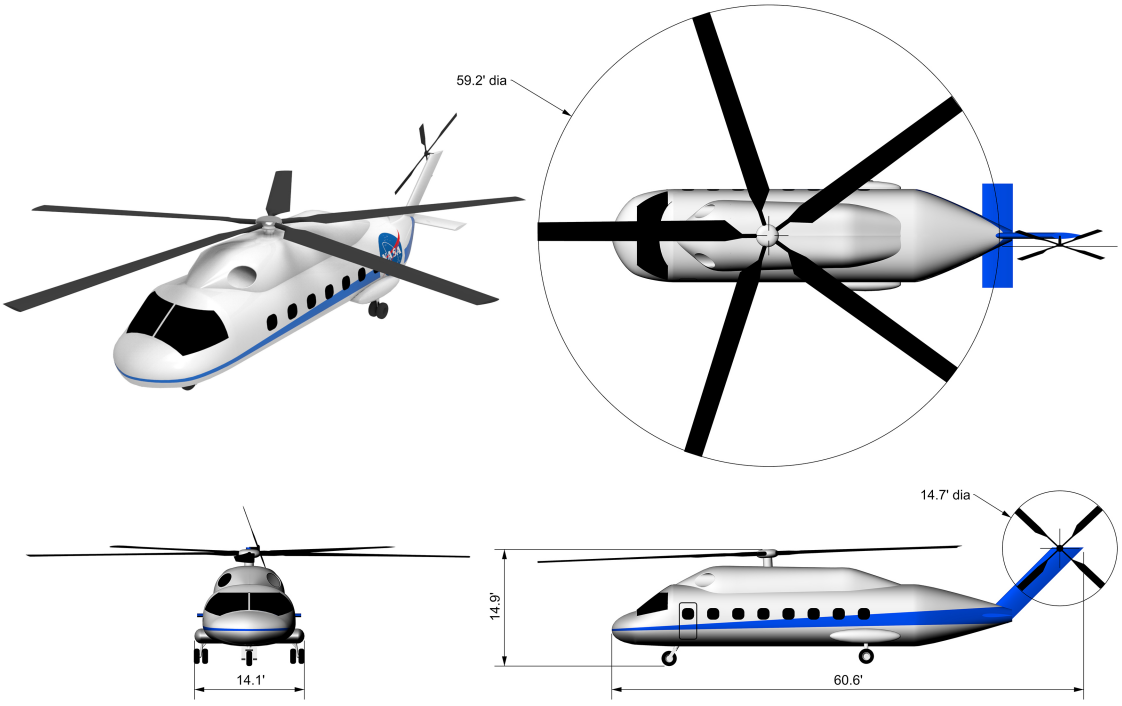

Fig. 24. Vehicle B Single Main Rotor Baseline

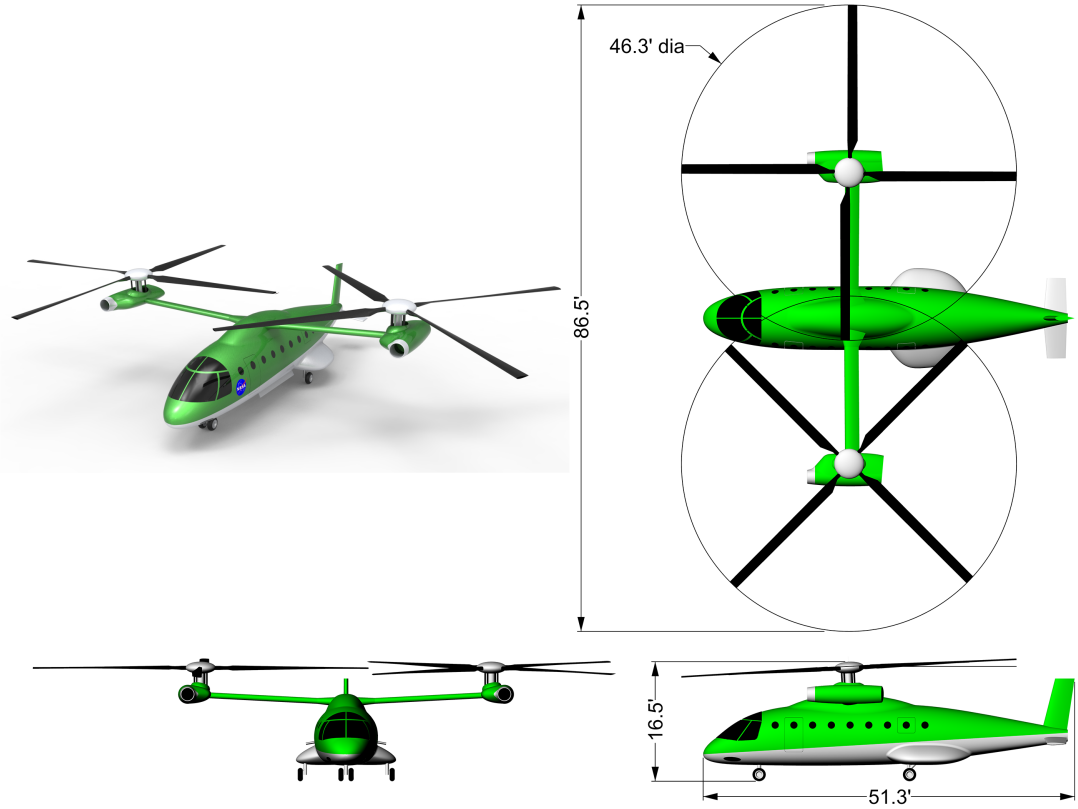

Fig. 25. Vehicle B Side-by-Side (Turboshaft)

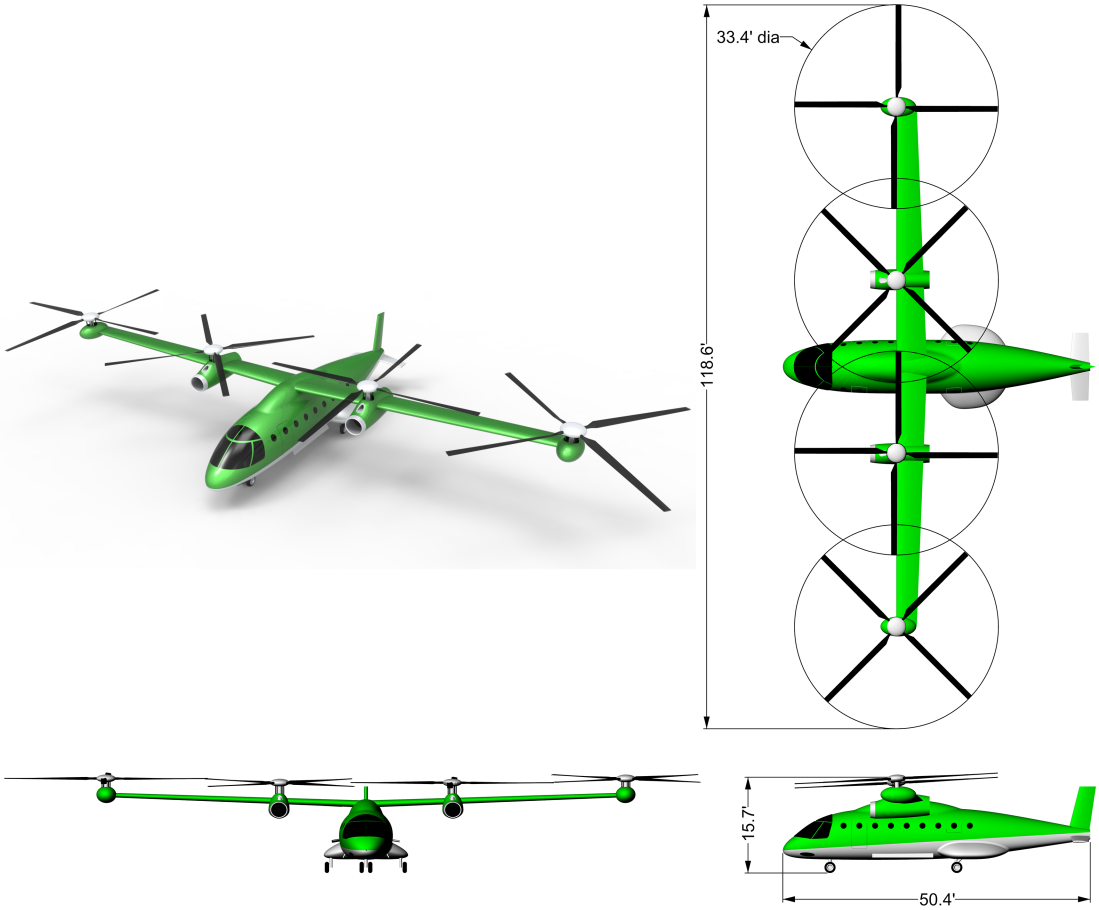

Fig. 26. Vehicle B 4x Side-by-Side (Turboshaft)

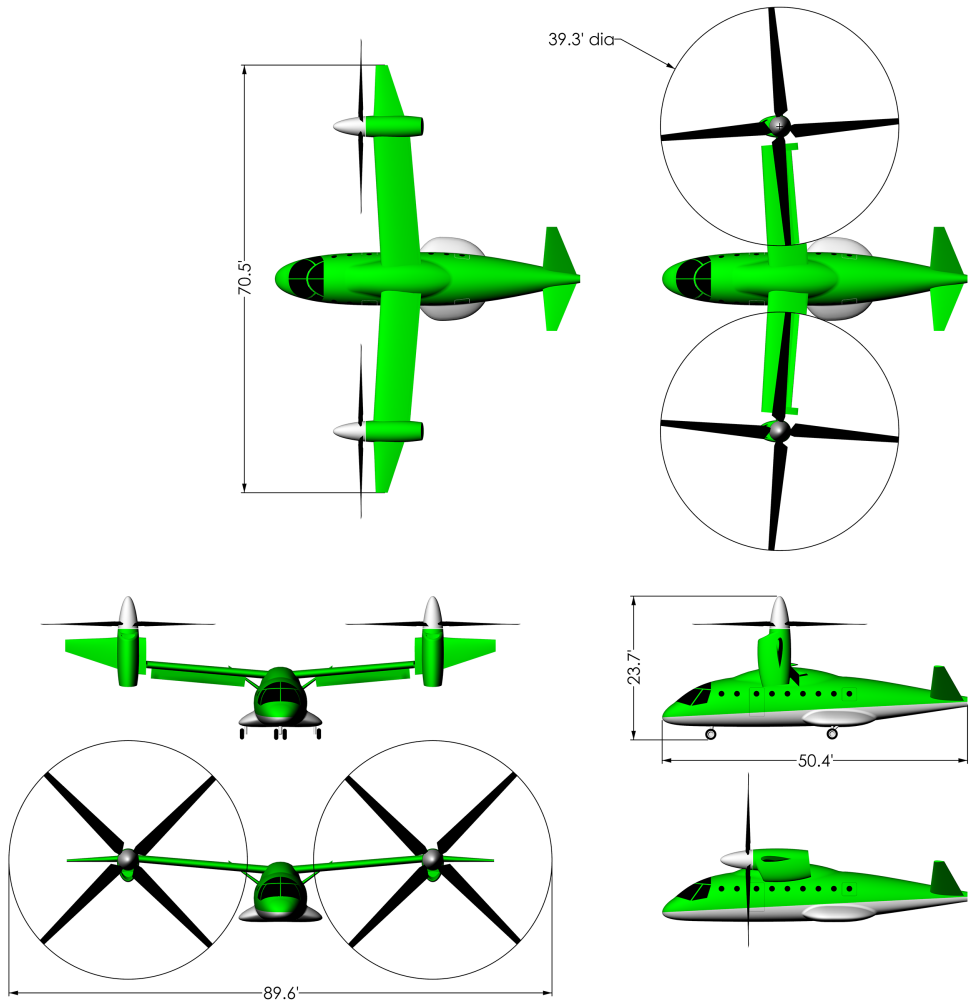

Fig. 27. Vehicle B High Efficiency Civil Tiltrotor (Turboshaft)

Fig. 28. Vehicle C Civil Tiltrotor Baseline

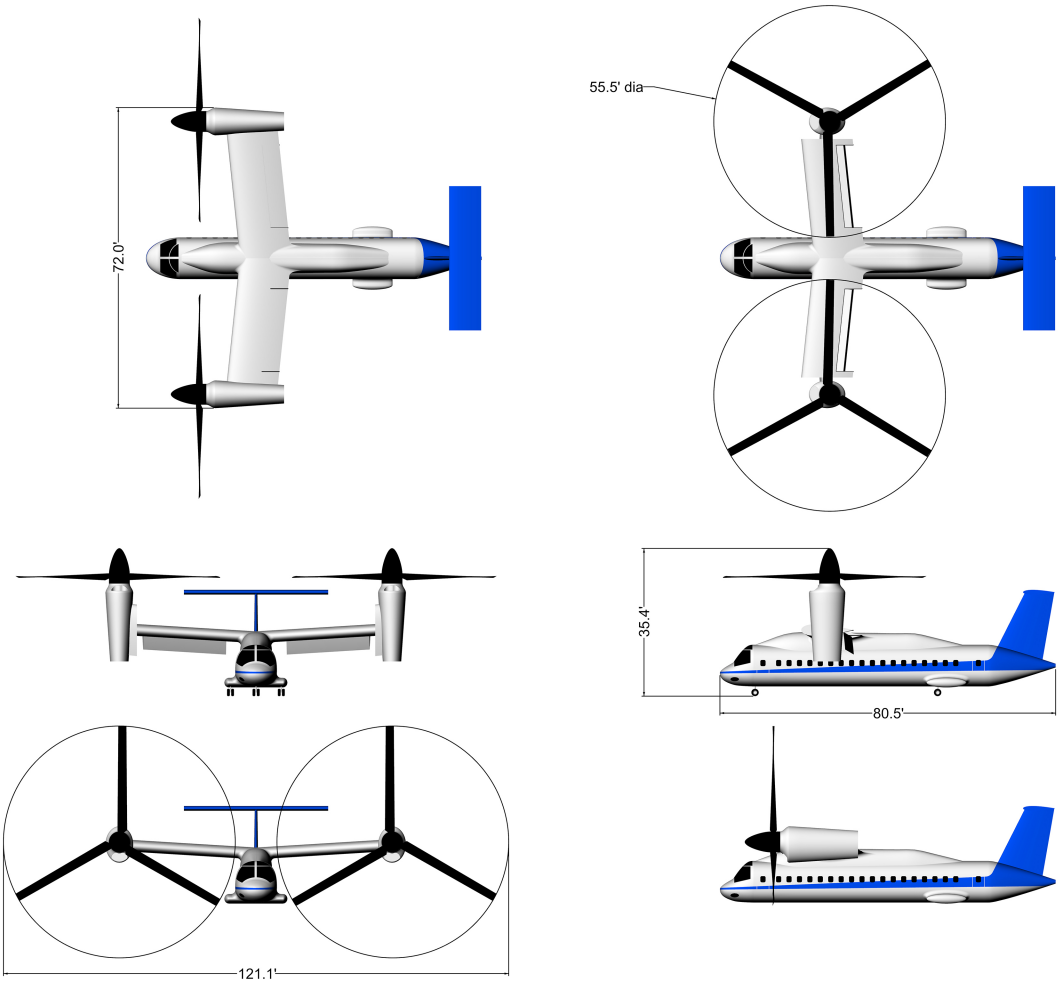

Fig. 29. Vehicle C Civil Tiltrotor Baseline

Fig. 30. Vehicle C High Efficiency Civil Tiltrotor (Turboshaft)

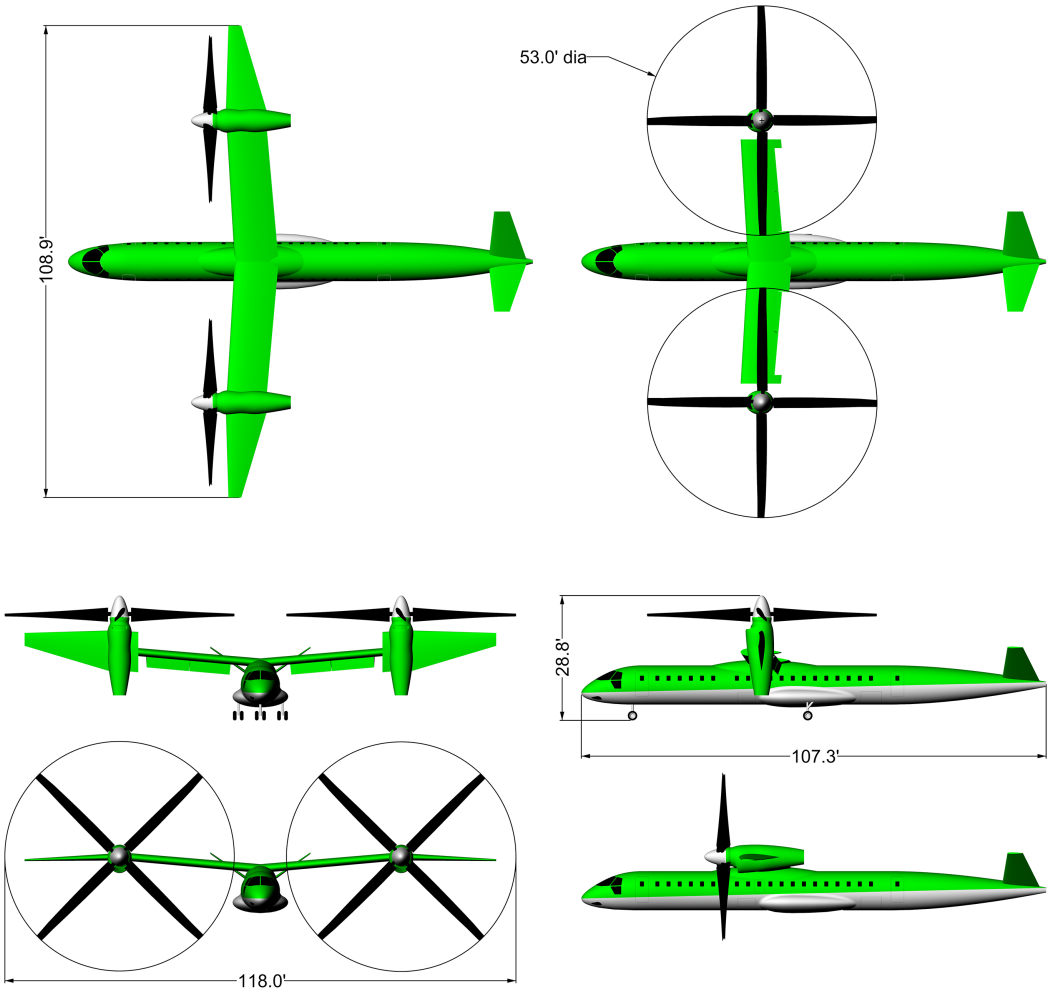

Fig. 31. Vehicle C High Efficiency Civil Tiltrotor (Turboshaft)